Manuscript Details

Manuscript number	ENGSTRUCT_2018_3984
Title	Advanced non-linear numerical modelling of masonry groin vaults of major historical importance: St. John Hospital case study in Jerusalem
Article type	Case study

Abstract

Three advanced non-linear modelling strategies for the evaluation of the non-linear behavior under horizontal loads of an historical groin vault in Jerusalem are presented. The vault presents the typical features of the Crusaders architecture, with masonry of the bearing structure, such as the piers and the main arches, made by big stocky stones with a high quality surface finish, and the vaults made with smaller irregular cobblestones. The first model is a FE Concrete Damage Plasticity FE-CDP macroscopic approach implemented in Abaqus where masonry is assumed elasto-plastic with damage in both tension and compression and scarcely resistant to tensile stresses. The second model is a non commercial Rigid Body and Spring RBS model, where the structure is discretized into rigid elements elasto-plastic with softening interfaces. Arches are modeled with a heterogeneous approach, whereas the vault itself by means of an isotropic material with quasi zero tensile strength and softening behavior. The last model is Kinematic Limit Analysis with adaptive mesh, constituted by few rigid infinitely resistant NURBS elements (NURBS-KLA). For validation purposes, an in-scale 1:5 model of the groin vault has been tested at the University of Florence under horizontal loads up to collapse, also in presence of FRP reinforcement, glued at the extrados after the activation of the collapse mechanism in the unreinforced case. Excellent agreement with experiments is obtained for all models, both in terms of load carrying capacity prediction and active failure mechanism, also in presence of FRP reinforcement, demonstrating the reliability of the procedures discussed.

Keywords	historical masonry groin vaults of major importance; advanced numerical modelling; heterogeneous damage-plasticity FE model FE-CDP; rigid body and spring RBS model; kinematic limit analysis with NURBS NURBS-KLA; validation against experiments; FRP strengthening
Taxonomy	Seismic Response, Seismic Vulnerability of Masonry Structures, Structural Engineering, Limit Analysis, Arch
Manuscript region of origin	Europe

Corresponding Author	Gabriele Milani
Corresponding Author's Institution	Technical University of Milan
Order of Authors	Gabriele Milani, marco valente, Mario Fagone, Tommaso Rotunno, Claudio Alessandri

Suggested reviewers	Vasilis Sarhosis, Andrea Chiozzi, Bahman Ghiassi, Elisa Bertolesi, Antonio Formisano

Submission Files Included in this PDF

File Name [File Type]

coverletter_ES_voltast_john.doc [Cover Letter]

highlights_ES_voltast_john.docx [Highlights]

Paper_stjohn_vfin-TM.docx [Manuscript File]

To view all the submission files, including those not included in the PDF, click on the manuscript title on your EVISE Homepage, then click 'Download zip file'.

Research Data Related to this Submission

There are no linked research data sets for this submission. The following reason is given:
Data will be made available on request

FROM:
Dr Gabriele Milani
Politecnico di Milano
Piazza Leonardo da Vinci 32
20133 Milano, Italy
e-mail: gabriele.milani@polimi.it

TO:
Engineering Structures

Tuesday, 18 December 2018

Dear Professor,

Please find enclosed the paper entitled:

"**Advanced non-linear numerical modelling of masonry groin vaults of major historical importance: St. John Hospital case study in Jerusalem**"

By Gabriele Milani, Marco Vincenzo Valente, Mario Fagone, Tommaso Rotunno, Claudio Alessandri

I would like to have the manuscript reviewed by your journal.

With the present, I hereby declare that:
1) The article is submitted for review only to your journal.
2) The article has not been already published.

Should you need to contact us, please use the above address.

Best Regards
Gabriele Milani

Highlights

- **Advanced numerical analysis of an historical masonry groin vault of major importance**
- **Detailed homogeneous 3D-FE approach with concrete damage plasticity CDP material**
- **rigid body and spring RBS model with heterogeneous lateral arches**
- **kinematic limit analysis KLA with few NURBS elements and progressive mesh adaptation**
- **comparison with 1:5 in scale model experimentally tested and FRP reinforcement**

Advanced non-linear numerical modelling of masonry groin vaults of major historical importance: St. John Hospital case study in Jerusalem

Gabriele MILANI *(1), Marco VALENTE (1), Mario FAGONE(2), Tommaso ROTUNNO(3), Claudio ALESSANDRI(4)

(1) Department of Architecture, Built environment and Construction engineering (ABC), Politecnico di Milano, Piazza Leonardo da Vinci 32, 20133, Milan (Italy)

(2) Dipartimento di Ingegneria Civile e Ambientale (DICeA), Università degli Studi di Firenze, Piazza Brunelleschi 6, 50121 Florence (Italy)

(3) Dipartimento di Architettura (DiDA), Università degli Studi di Firenze, Piazza Brunelleschi 6, 50121 Florence (Italy)

(4) Department of Engineering, University of Ferrara, Via Saragat 1, 44100 Ferrara (Italy)

* corresponding author, e-mail: gabriele.milani@polimi.it

Abstract

Three advanced non-linear modelling strategies for the evaluation of the non-linear behavior under horizontal loads of an historical groin vault in Jerusalem are presented. The vault presents the typical features of the Crusaders architecture, with masonry of the bearing structure, such as the piers and the main arches, made by big stocky stones with a high quality surface finish, and the vaults made with smaller irregular cobblestones. The first model is a FE Concrete Damage Plasticity FE-CDP macroscopic approach implemented in Abaqus where masonry is assumed elasto-plastic with damage in both tension and compression and scarcely resistant to tensile stresses. The second model is a non commercial Rigid Body and Spring RBS model, where the structure is discretized into rigid elements elasto-plastic with softening interfaces. Arches are modeled with a heterogeneous approach, whereas the vault itself by means of an isotropic material with quasi zero tensile strength and softening behavior. The last model is Kinematic Limit Analysis with adaptive mesh, constituted by few rigid infinitely resistant NURBS elements (NURBS-KLA). For validation purposes, an in-scale 1:5 model of the groin vault has been tested at the University of Florence under horizontal loads up to collapse, also in presence of FRP reinforcement, glued at the extrados after the activation of the collapse mechanism in the unreinforced case. Excellent agreement with experiments is obtained for all models, both in terms of load carrying capacity prediction and active failure mechanism, also in presence of FRP reinforcement, demonstrating the reliability of the procedures discussed.

Keywords: historical masonry groin vaults of major importance; advanced numerical modelling; homogeneous damage-plasticity FE model FE-CDP; rigid body and spring RBS model with heterogeneous lateral arches; kinematic limit analysis with NURBS NURBS-KLA; validation against experiments; FRP strengthening

1 Introduction

The evaluation of the ultimate load bearing capacity and displacement capacity of historical masonry vaults under horizontal loads by means of sophisticated numerical approaches is particularly needed for a reliable prediction of their vulnerability [1–14]. In addition, the knowledge of the actual failure mechanism associated to the collapse state is paramount to design a strengthening intervention [15–19] that is effective and, hence, able to considerably increase the load carrying capacity [20–24].

The present research focuses on a prestigious case study, namely a groin vault in St. John Hospital in Jerusalem, and discusses the capabilities of three advanced numerical approaches in predicting the seismic behavior of historical double curvature structures exhibiting uncommon complexity.

The building of St. John Hospital, partially owned by the Order of St. John, is located in the Old City of Jerusalem and is one of the few standing remains of the St. John Hospital complex, erected by the Crusaders at the beginning of the 12th century and belonging to a larger quarter, the so called Hospitallers quarter, including monasteries, churches, bathhouses, the knights' dormitory and refectory, granary, stables and hospitalities facilities for pilgrims. By the end of the 12th century the quarter took its definite structure: a group of monumental Romanesque groin-vaulted halls (Figure 1), served by a network of narrow streets with barrel-vaulted shops and stores. Over the course of nearly three centuries, Muslim and Christian pilgrims continued to be assisted and cared of inside the St. John Hospital. By the 17th century, however, it fell into ruins. Nowadays, despite its past history and peculiar position in the very heart of the City, the building is largely under-utilized, since it serves only as storage for the adjacent shops.

The building is composed of ten groin vaults organized on three lines, see Figure 2; the vaults present the typical features of the Crusaders buildings: the masonry of the bearing structure, such as the piers and the main arches, is made of great squared stones with a high quality surface finish, whereas the vaults themselves are made with smaller and more irregular stones, to be covered by plasters. Such vaults have average span and crown height from the ground respectively equal to 4.5 and 4 meters, while the piers are quite stocky and have an average width and height equal to 1.5 meters, as visible from photos reported in Figure 1. The current material and structural conditions of the building do not present significant damage pathologies. There is an advanced state of deterioration on the external surfaces as a result of the demolition of higher levels and the consequent exposure to erosion due to winds and rain water, which in any case could have harmful effects on the structural parts in the future.

Jerusalem is however in seismic zone 2A according to Palestine seismic hazard, with a non-negligible PGA of 0.15g. The preservation of such complex structural elements, in view also of their historical and archaeological importance, needs therefore non standard numerical modelling with proved reliability, and this issue is discussed in the present paper.

(a)\ (b)

Figure 1: The existing groin vaults in St. John Hospital. Details of the vaulted structures (a) and of the lateral arches (b).

Another important argument corroborates the need to arrange a set of numerical tools robust and reliable to predict the structural behavior of such vaults. Indeed, in view of its historical significance, architectonic features and strategic position in the heart of the old city, UNESCO has included the St. John Hospital in a list of buildings subjected to "Adaptive reuse projects", as described in UNESCO Action Plan for the Safeguarding of the Cultural Heritage of the Old City of Jerusalem [25]. The project profiles described in the Action Plan include architectural surveys and structural analyses at different scale and an early assessment of the structural condition, mainly aimed at the evaluation of the possible reuse options. In particular, conservation interventions have been recommended for the St. John Hospital, in order to preserve, reinforce, and restore the structures of the building.

Considering in particular such a need, three advanced numerical methods applicable to the seismic assessment and vulnerability reduction of groin vaults of major importance are here discussed and critically compared. The paper focuses on the aforementioned prestigious case study, but software adopted are sufficiently versatile to recommend their application to different vaulted systems. It is important to underline, indeed, that the typology of the vaults of St. John Hospital is among the most frequent in the medieval architecture of many of the Middle-Eastern Countries, once occupied by the Crusaders. Therefore, it is straightforward to infer that the approaches here adopted could be also extended at least to similar vaulted structures of that area. Among the main characteristics of these vaults it is necessary to mention the height of the vault crown that is slightly higher than the one of the key stones of the lateral arches. Moreover, the latter are made of squared stones with different dimensions that alternate with regularity in order to allow a better grip with the masonry of the vaults.

The first numerical model is a finite element concrete damage plasticity (hereafter called FE-CDP) macroscopic approach implemented in Abaqus [26], where lateral arches and the central vault are discretized with 4-noded tetrahedron elements. Vault is assumed to behave isotropically, with an elasto-plastic behavior and distinct damage parameters in tension and compression. Tensile strength

is assumed almost vanishing, so approximating the no-tension material hypothesis [27] For lateral arches, a homogeneous elastic material unable to withstand tensile stresses is assumed. Despite a heterogeneous approach would be more close to the real behavior of the arches, which fail for the formation of hinges located inside thin mortar joints, it has been proved [28–32] that the approximation with a no-tension material (i.e. without distinction between joints and stones) still provides very good results, especially if the span of the arch is much larger than the block dimensions). The second model is a non-commercial Rigid Body and Spring model (hereafter called RBS for the sake of brevity). It belongs to the wide family of discrete approaches [29-37]*)*, a class including the distinct element method DEM [10], mixed FEM/DEM, RBSM [42–44], peri-dynamics and many others. In this case, the vault is discretized into rigid triangular elements and elasto-plastic with softening interfaces, whereas arches are modeled with a heterogeneous approach. The material model assumed for the vault is isotropic with quasi zero tensile strength and softening behavior in both tension and compression. The utilization of an isotropic material is justified by the irregularity of the stones used to build the vault. Anyway, in all those cases where it would be needed, a homogenization procedure could be used prior structural analyses, to calibrate the orthotropic properties to adopt for triangle-triangle interfaces [45–47]. The last modelling approach is an upper bound (kinematic) limit analysis with adaptive mesh, constituted by few rigid infinitely resistant NURBS elements interconnected by homogenized rigid-plastic curved interfaces. For the sake of conciseness, the acronym NURBS-KLA (Kinematic Limit Analysis) is used from here ongoing. NURBS-KLA has already been validated for masonry vaults on a number of different benchmarks against a variety of available alternative approaches (the interested reader is referred to [21][48]). The most important advantage is that few elements are needed to discretize very precisely complex geometries; furthermore, shape and position of the interfaces are quickly adjusted step by step to closely reproduce the active failure mechanism. Whilst limit analysis does not allow any prediction of both displacements near failure and post peak behavior, it furnishes with a quite limited computational effort collapse loads and active mechanisms, suggesting therefore the most suitable strengthening to implement in view of a refurbishment or a vulnerability reduction.

Numerical data are validated by means of experimental analyses carried out in the “Laboratorio Ufficiale Prove Materiali e Strutture” of the Department of Architecture (University of Florence - Italy) on in-scale models. In particular, a 1:5 in-scale vault reproducing closely the real geometry is tested under an increasing horizontal force positioned on the keystone of one lateral arch up to the activation of a failure mechanism. A strengthening with Carbon Fiber Reinforced Polymers (CFRP) is then applied on the collapsed vault, with the aim of evaluating the effectiveness of a well-known

consolidation system used in reducing the vulnerability, in light of its practical implementation to a sample of the St. John Hospital.

Bonding CFRP strips at the extrados of masonry vaulted structures is well-established in common practice, but it is only partially standardized (some issues are still open, as for instance delamination on curved surfaces [49–52]) and there are still few specialized numerical tools able to suitably take into account different important aspects, such as delamination from brittle supports, influence of masonry texture, anchorage strength and effect induced by the curvature. In the three numerical approaches here proposed, all these aspects have been properly taken into account and extensive validations on different structural elements are available from the literature, see for instance. In FE-CDP and RBS approaches, FRP strips are modeled with equivalent trusses with fictitious tensile strength and softening behavior, both tuned according to the Italian technical recommendations for FRP strengthening (CNR DT200 [53]); consistently with this, delamination peak strength and fracture energy after delamination are accounted for in a conventional but effective way. In NURBS-KLA (third model) the same concept is followed, but obviously assuming trusses as rigid-perfectly plastic, as required by classic limit analysis.

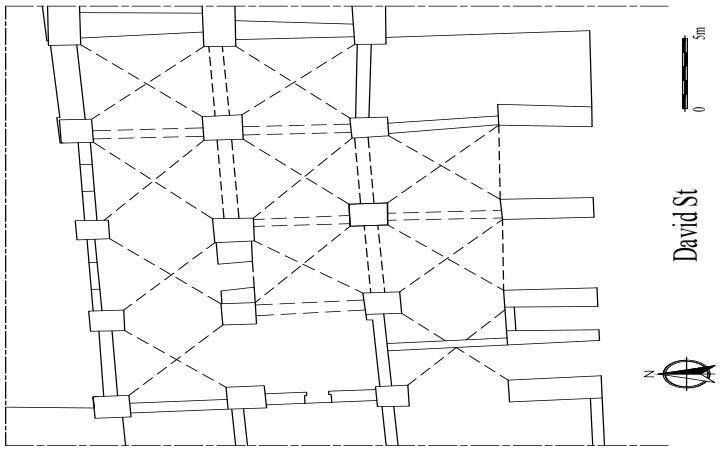

Figure 2: The groin vault system of St. John Hospital; plane view.

All models proved to be reliable also in presence of FRP, giving a realistic information on the structural role played by the reinforcement system, namely the inhibition of the unreinforced case failure mechanism with the activation of another mechanism associated to a higher collapse load. For the first two-models, an excellent prediction of the post-peak behavior was also obtained.

The paper is organized as follows: in Section 2, the in-scale model of the groin vault tested at the University of Florence is presented and experimental results in absence and presence of reinforcement are discussed in detail. Section 3 comprehensively presents the three numerical models adopted (FE-CDP, RBS and NURBS-KLA), focusing in particular on masonry softening behavior and on the implementation of FRP elements.

In Section 4, the numerical results obtained are compared and critically commented, highlighting possibilities and limitations of the different approaches. Finally Section 5 is devoted to draw conclusions on the experiences collected in the numerical modelling phase of the complex case study discussed.

2 The vault experimentally analyzed

In order to validate the different numerical approaches proposed in the following Section, a comprehensive experimental investigation on a 1:5 scale model of a single groin vault, representative of the groin vault system of St John Hospital, has been carried out at the University of Florence and fully described in [54]. Here a short overview of the mechanical characterization on the materials carried out and the most relevant results obtained on the vaults with the application of a concentrated horizontal load and the subsequent reinforcement with FRP after the activation of a failure mechanism are provided.

The geometric characteristics of the scale model, reported in Figure 3, have been determined as the average values of the dimensions of the real system.

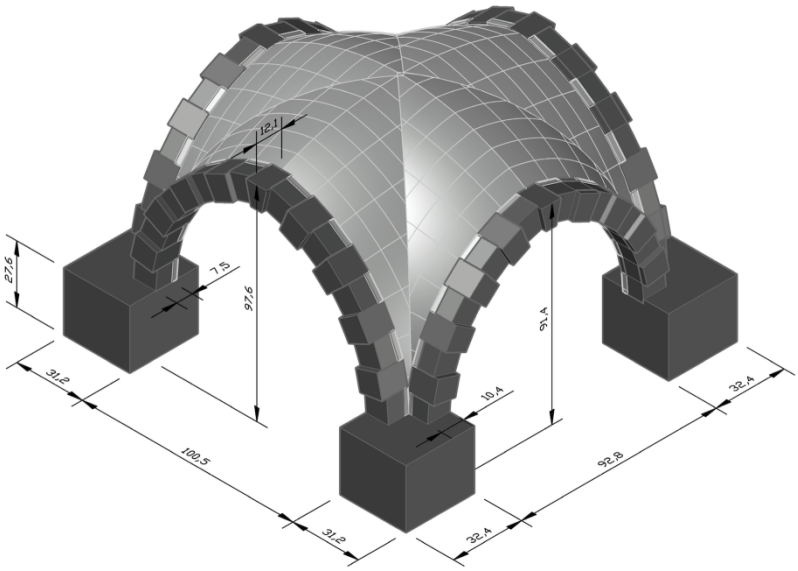

Figure 3: The 1:5 scale vault tested at the University of Florence (measures in cm).

The model was manufactured using cement-lime mortar and a sandstone (“Pietra Alberese”), whose main mechanical properties, obtained by ad hoc experimental program, are summarized in Table 1. The CFRP sheet reinforcement system consisted of a layer of a single-direction carbon fibers fabric and two layers of two-component epoxy-base adhesive, applied according to the manufacturer indications using a wet lay-up procedure. Physical and mechanical properties of the fiber and the adhesive are reported in Table 2.

Table 1: Mechanical properties of "Pietra Alberese" and cement-lime mortar.

Material	**Property**	**# specimens**	**Average value [MPa]**
Pietra Alberese	Compressive strength[(a)]	6	97.3
	Indirect tensile strength[(b)]	6	6.6
cement-lime mortar	Compressive strength[(c)]	6	6.40
	Bending tensile strength[(c)]	3	1.75

[a] according to EN 1926 (2006)
[b] according to ASTM C496/C496M-11 (2004)
[c] according to UNI EN 1015-11 (2007)

Table 2: Technical specifications of the reinforcing system producer.

Property	**Fiber**	**Adhesive**
Areal weight (g/m^2)	310 ± 10	-
Bulk density (kg/liter)	-	1.04 ± 0.05
Tension Young's modulus (MPa)	194000	2590
Direct tensile strength (MPa)	2750	34.6
Ultimate strain (%)	1.4	1.8

However, it is worth mentioning that, in order to set correctly mechanical properties of any numerical model usable to fit experimental data, the most important parameter to characterize is the bond behavior between mortar and stones. It is usually dominated by an almost vanishing tensile strength, which here has been determined experimentally by direct tensile tests performed on specimens constituted by two parallelepiped stones with square cross section of edge length equal to 55 mm and height equal to 80 mm, bonded by mortar 5 mm thick, see Figure 4. Five replicates have been tested, with specimens prepared after wetting properly stones and a maturing period of 28 days. Results indicate a failure mode characterize by a planar smooth crack at the interface between mortar and block, see Figure 4(d) and a very small tensile strength, on average equal to 0.01 MPa (cov 7.11%). Mechanical properties to adopt in the numerical models in tension for the masonry material are therefore those of the interface between mortar and blocks, which is clearly characterized by a strength in tension almost vanishing (quasi no tension material modelling).

(a) (b)

Figure 4: Specimens used to characterize the bond behavior between mortar and stones through direct tensile tests. (a) specimens tested. (b) direct tensile tests performed. (c) crack pattern at failure and (d) detail of the detachment interface.

As far as the in-scale groin vault tests are concerned, the (unreinforced) model was loaded by a constant vertical load and by a cyclic horizontal load. Then, the damaged scale model was reinforced with continuous CFRP strips bonded at the extrados (see Figure 5) and tested again applying a similar load history. In particular, in both tests the constant vertical load was equal to 9 kN, uniformly distributed at the extrados surface of the vault, while the horizontal load was applied, using a hydraulic jack, at the keystone of one of the wall arches, as depicted in Figure 6. Four load cycles were carried out on the unreinforced vault: the first ranging between 0 and 1.00 kN, the second between 0 and 2.00 kN, the third between 0 and 3.00 kN and the fourth between zero and the peak load, which was reached at 3.50 kN. Similarly, three load cycles were performed on the reinforced vault: the first ranging between 0 and 1.50 kN, the second between 0 and 3.50 kN (corresponding to the peak load of unreinforced model), the third between 0 and the peak load, which was reached at 5.10 kN.

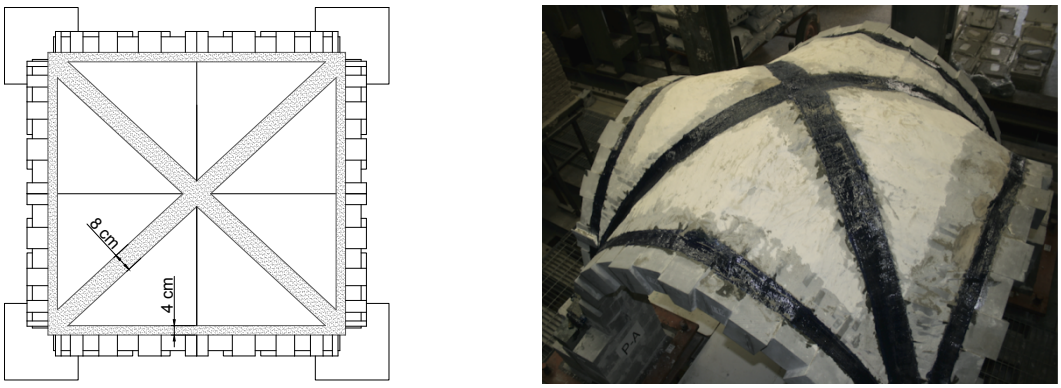

(a) (b)

Figure 5: Geometric characteristics of the CFRP sheet reinforcement.

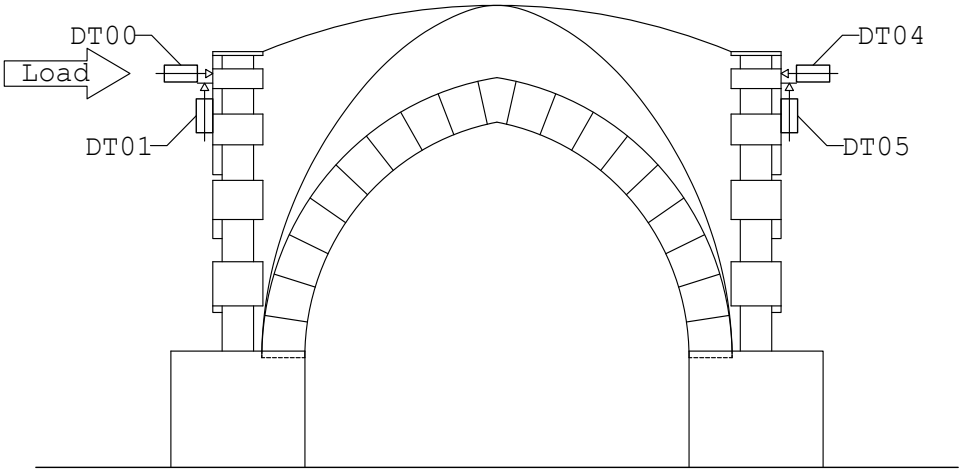

Figure 6: Displacement transducers monitoring the vertical and horizontal displacement of the keystones

The vertical and horizontal displacements of the keystones of the wall arches orthogonal to the load direction, measured by the displacement transducers (DT00, 01, 04 and 05) positioned as described Figure 6, have been used to compare the numerical and the experimental results.

The experimental load-displacement diagrams referring to the unreinforced vault are reported in Figure 7. It is interesting to point out that, at least until the peak load, the vertical displacements of the keystones (see DT00 measurements compared with the others) have opposite sign, clearly indicating a rotation of the vault around a horizontal axis, orthogonal to the load direction. Within the load cycles the diagrams show irreversible displacements. Moreover, it appears clearly that, after the first load cycle (maximum load equal to 1.00 kN) the residual horizontal displacement was almost zero, whereas it increased considerably in the successive cycles, characterized by higher maximum loads. After the peak load, the displacements increased with almost constant load, meaning that the activation of a failure mechanism has been reached. Major crack locations (not indicating the whole failure mechanism active) observed experimentally and corresponding to the last load step following

the peak load before unloading, are reported in Figure 8. Authors experienced also that at the end of the test, the most damaged areas of the model were all localized on the springing, close to the pillars.

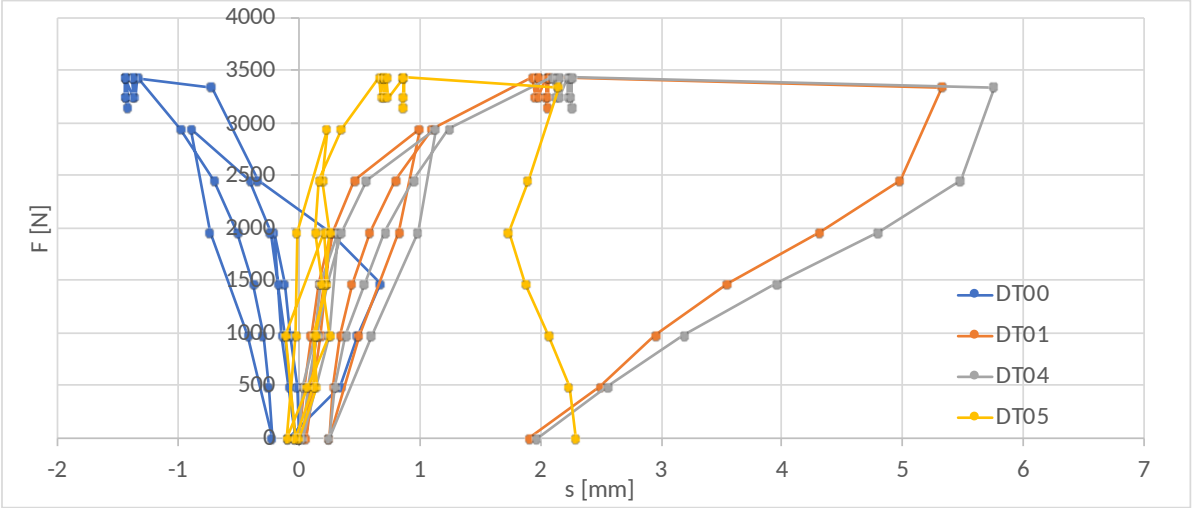

Figure 7: Unreinforced vault: load-vertical displacement diagrams.

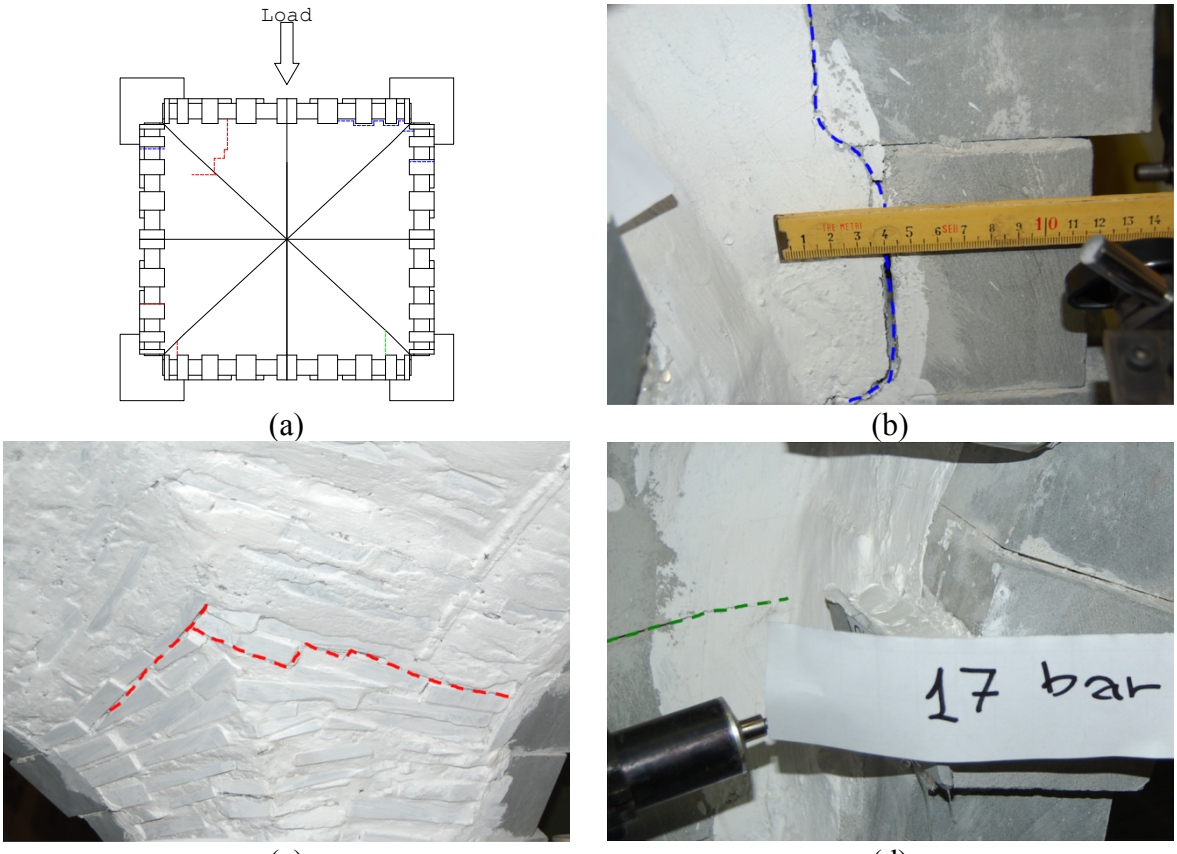

(a) (b)

(c) (d)

Figure 8: a) Crack locations: intrados crack (red), extrados crack (green), through-thickness crack (blue); b), c) and d) Crack details.

The load-displacement diagrams obtained from the test carried out on the reinforced vault are reported in Figure 9. As can be noted, at least until the peak load is reached, the vertical displacements of the keystones are much smaller than those measured for the unreinforced model. The vertical

displacements of the keystones have similar initial path, corresponding to almost rigid vertical translation of the vault, followed by a rotation of the vault around a horizontal axis orthogonal to the direction of the load. After unloading, not negligible residual displacements were recorded.
Moreover, after the first two load cycles, negligible residual horizontal displacements were observed, the scale model showing an almost reversible behavior (i.e. the entire structure essentially remained in the linear elastic range). Increasing the displacement applied to the model, after reaching the peak, load sharply decreased highlighting a considerable damage of the vault prototype; increasing further the displacement, the load remained quasi-constant up to the beginning of the unloading phase.
Moreover, crack locations reported in Figure 10 show that major fractures were located exclusively in correspondence of the pillars, highlighting a monolithic behavior of the strengthened vault.

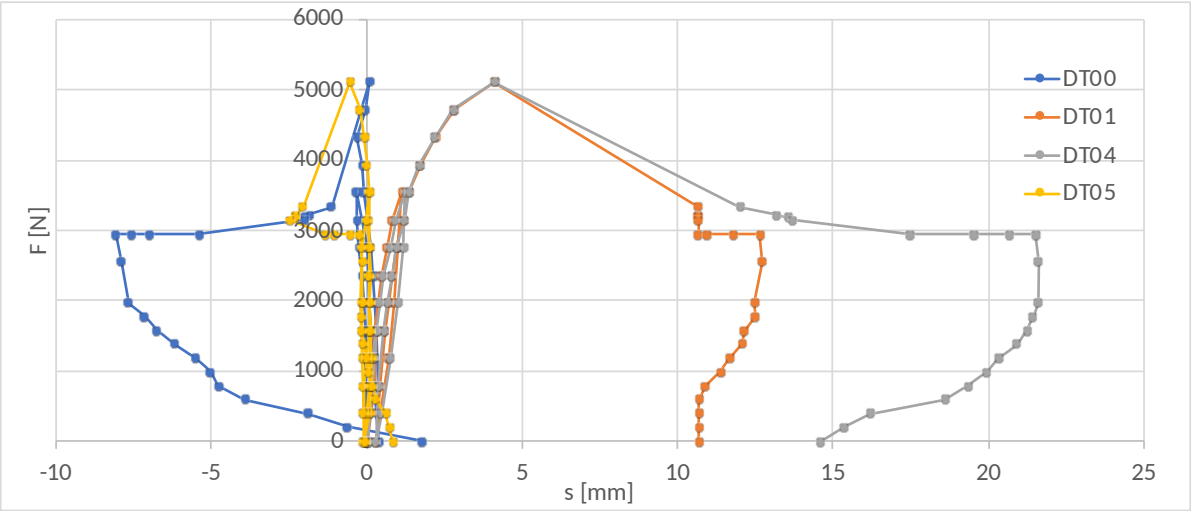

Figure 9: Reinforced vault: load-displacement diagrams.

3 The numerical models used

In the present Section, an overview of the models proposed is provided. Basically, two different approaches are utilized: 1) a FE Abaqus approach where masonry is modeled as a Concrete Damage Plasticity CDP material (FE-CDP model); 2) a Rigid Body and Spring RBS approach with rigid elements and inelastic interfaces characterized by a step by step solution found with mathematical programming (in particular Sequential Quadratic Programming SQP), where the vault is modeled as a homogeneous isotropic material with softening, whereas boundary arches are modeled with a heterogeneous procedure with infinitely resistant and stiff blocks and joints are reduced to interfaces where elastic and inelastic deformation is lumped; 3) an Upper Bound Limit analysis where meshes used are constituted by few NURBS elements whose shape is sequentially adapted by means of an efficient Genetic Algorithm approach.

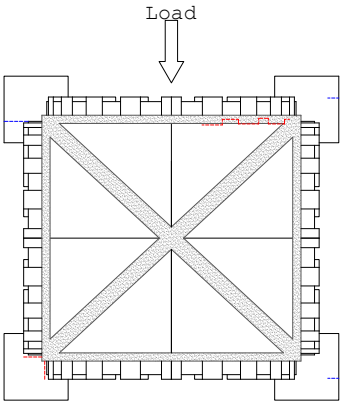

(a)

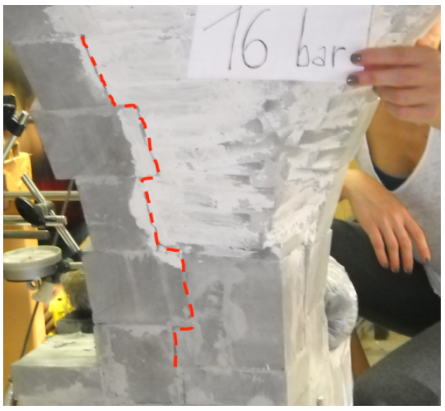

(b)

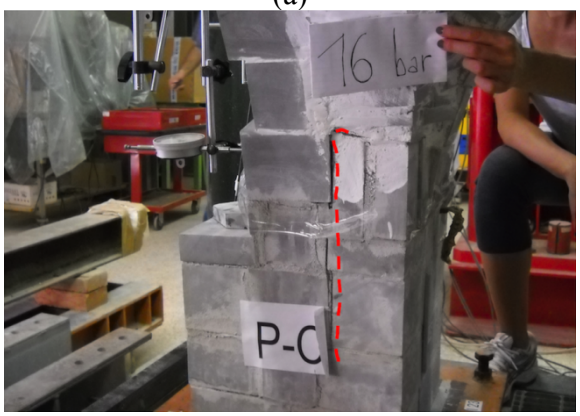

(c)

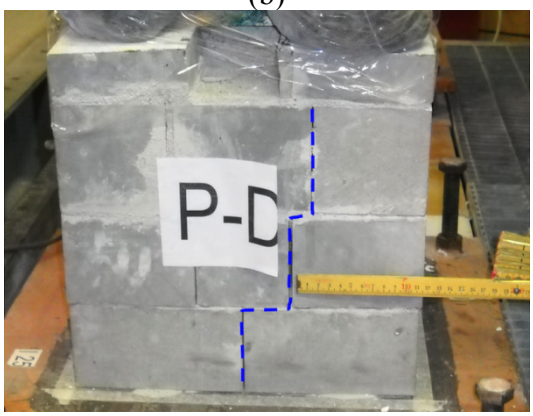

(d)

Figure 10: Crack locations: intrados crack (red); through-thickness crack (blue); b), c) and d) Crack details.

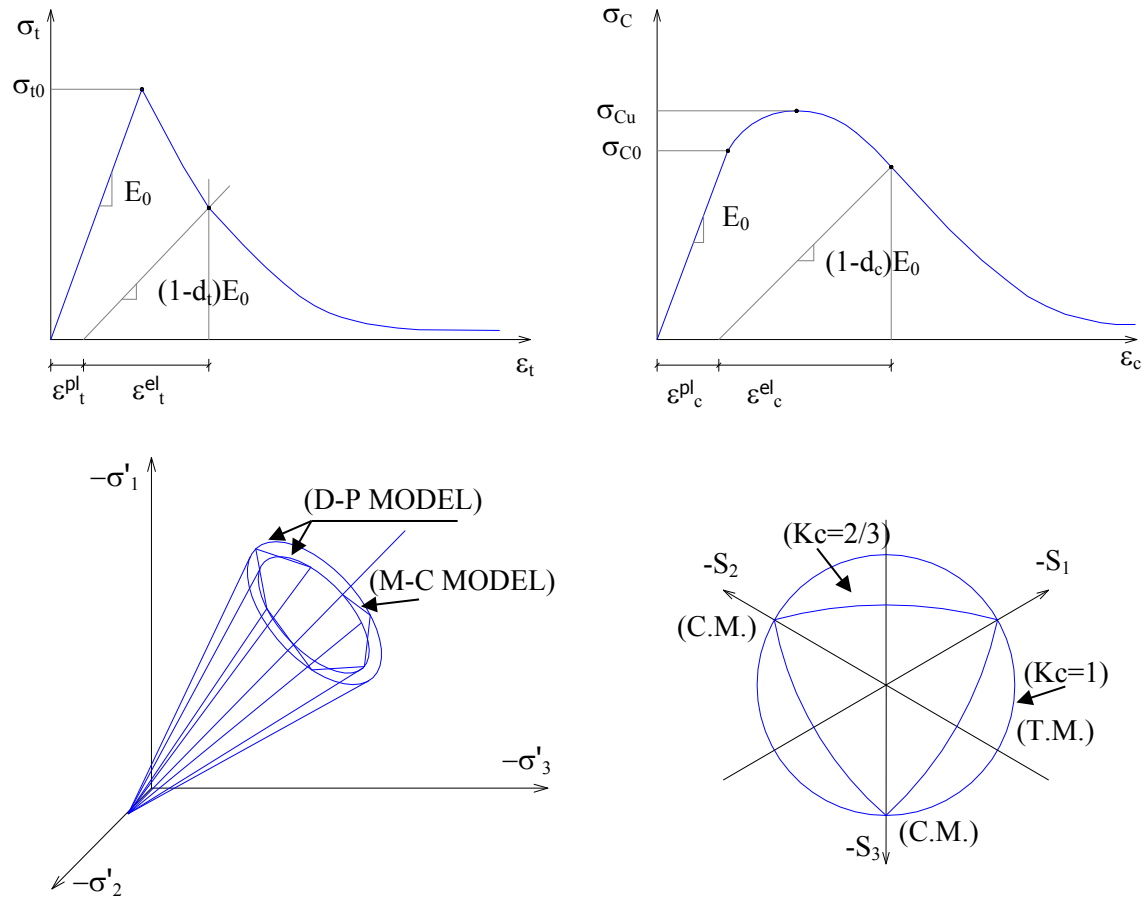

Figure 11: ABAQUS material non-linear behavior in uniaxial tension and compression to analyze the bell tower under non-linear dynamic loads.

3.1 FE CDP model

The so called Concrete Damage Plasticity (CDP) model utilized for analysing numerically the vault is a tool already available in the Abaqus [26] standard software package. Although the model was conceived by Lubliner and co-workers in [55] specifically to deal with concrete, it owns all the necessary basic features needed to be successfully adopted for advanced macroscopic computations on masonry structural elements. As a matter of fact, it is specifically suited for a fragile isotropic material like concrete, because it allows for modelling materials with distinct tensile and compressive strengths, different post peak behaviors, distinct damage parameters and a cohesive frictional material under shear actions, as sketched in Figure 11. Consequently, its basic constitutive laws can be adapted easily for reproducing suitably masonry properties at the macro scale. Orthotropy is lost, because CDP is strictly isotropic, but this is not necessary a limitation in this specific case, because, whilst CDP should be in principle avoided for regular arrangements of blocks, when masonry is an

assemblage of irregular stones, pebbles and mortar (as is the case here treated, at least for the internal vault) orthotropy becomes irrelevant (as shown for instance in [56,57]) and an isotropic model becomes perfectly suitable.

The model assumes that the total strain is constituted by three components, one elastic and two inelastic, corresponding respectively to the plastic and the damaging part. In this way, CDP becomes extremely precise in fitting load-unload tests on masonry, where cracking and crushing are due to the combined increase of damage and plastic deformation. Under cyclic loading conditions the degradation mechanisms involve the opening and closing of previously formed cracks. The experimentally observed effect, according to which there is some recovery of the elastic stiffness as the stress changes sign, is called "unilateral effect". This phenomenon, which is usually more pronounced as the stress state changes from tension to compression, causing tensile cracks to close, can be easily modelled by two distinct damage variables, one in compression and one in tension, which are assumed to be function of the plastic strains. These variables may assume values from zero (undamaged material) to one, the latter corresponding to a total loss of stiffness.

Table 3: Additional CDP parameters adopted in the numerical simulations

Ψ [°]	K_c	e	f_{b0}/f_{c0}	μ
Dilatance angle	DP correction parameter	eccentricity	Biaxial strength ratio	Viscosity parameters
10	0.666	0.1	1.16	0.02

The strength domain is a Drucker Prager DP surface eventually modified by a parameter K_c, which has the role to smoothly distort the DP surface in the deviatoric plane from a circle to a surface more similar to a Mohr-Coulomb one. K_c physically represents the ratio between distance from the hydrostatic axis of the maximum compression and tension respectively. In the simulations reported hereafter, K_c (Table 3) has been kept equal to 2/3, a value suggested by the user's Guide to well approximate a Mohr-Coulomb failure criterion.

A regularization of the tensile corner is also adopted in the model, approximating in the p-q plane the line representing the DP domain with a hyperbola. Regularization is practically obtained in the model with a further correction parameter, referred to as eccentricity e, expressing the rate at which the plastic flow potential approaches the linear Drucker-Prager function at high confining pressure stress. The 0.1 default value was adopted, see Table 3. Smaller values may cause convergence problems when the material is subjected to low confining pressures because of the very tight curvature the flow potential possesses locally where it intersects the hydrostatic axis. Such choice turns out to be responsible for a decrease of the tensile strength, but with an acceptable error lower than 5%.

Another important issue dealing with masonry is the non-associativity of the plastic part. CDP allows to set a user defined dilatance angle of the elasto-plastic part of the inelastic deformation, which is usually kept equal to 10° (Table 3), in agreement with some experimental data by van der Pluijm [58,59] in presence of moderate pre-compression levels. Indeed, dilatance changes considerably varying the level of normal stress during a shear deformation and a value of 10° corresponds to joints subjected to average levels of pre-compression.

A value equal to 1.16 (Table 3) describing the ratio between the biaxial and monoaxial compression strength has been adopted, again in agreement with consolidated literature regarding the behavior of clay-brick masonry in biaxial compression [60–62]. Finally, a relatively large value (albeit in the ranges suggested by the user's manual) of viscosity parameter has been adopted to promote faster convergence in presence of several elements in the softening branch.

The uniaxial inelastic behavior due to the damage part is evaluated with a multi-linear softening model in both tension and compression, with strains depurated from the elastic part.

Values adopted in the model are summarized in Table 4 and Table 5 for the tensile and compressive behavior respectively and they are kept, were possible, in agreement with experimental data obtained during the characterization of the materials, see previous Section.

Table 4: Mechanical properties adopted in the CDP model for vault and lateral arches and pillars

Vault				Lateral arches and pillars			
f_c [MPa]	**E [MPa]**	**τ_0 [MPa]**	**G [MPa]**	**f_c [MPa]**	**E [MPa]**	**f_t [MPa]**	**G [MPa]**
2.2	900	0.04	190	6.29	1429	0.12	389

Table 5: Relation between damages in tension and compression and inelastic strains

Compression		**Tension**	
d_c	**Anelastic strain**	**d_t**	**Anelastic strain**
0	0	0	0
0.95	0.033	0.95	0.002

Damage parameters d_t e d_c in tension and compression enter, as usual, into the uniaxial Hook's law as $\sigma_t = (1-d_t) E_0 \left(\varepsilon_t - \varepsilon_t^{ple}\right)$ and $\sigma_c = (1-d_c) E_0 \left(\varepsilon_c - \varepsilon_c^{ple}\right)$ where σ_t and σ_c are uniaxial tensile and compressive stresses, E_0 is the initial elastic modulus, ε_c and ε_t are the total strain in compression and tension and ε_c^{ple} (ε_t^{ple}) are the total plastic deformation in compression (tension).

3.2 Rigid Body and Spring (RBS) approach

The numerical analyses are carried out by means of a non-linear FE homogenized and heterogeneous software implemented by one of the authors. Originally the code was conceived for the homogenized limit analysis of both masonry curved structures and arch bridges (e.g. [63,64]), in presence of materials exhibiting low tensile strength and softening. In [65] the model was extended to a heterogeneous approach (i.e. distinct mesh between mortar and bricks) and the introduction of FRP reinforcement is possible as well, as shown by simulations reported in [66].

In the model, masonry (or stones/blocks/bricks when a heterogeneous approach is used) is dicretized by means of rigid-infinitely resistant 6 nodes elements connected by elasto-plastic interfaces with softening. The continuum is characterized by a plate and shell behavior, with possibility to consider out-of-plane sliding (thick plate hypothesis).

In the present case, edge arches are modelled meshing separately each block by means of rigid infinitely resistant beam elements with possible plasticization at the interfaces. In order to take into account all possible failure modes between two blocks of the arch, instead of using flexural hinges quadrilateral interfaces are considered with tangential and normal springs placed on Gauss Points, as schematically shown in Figure 12.

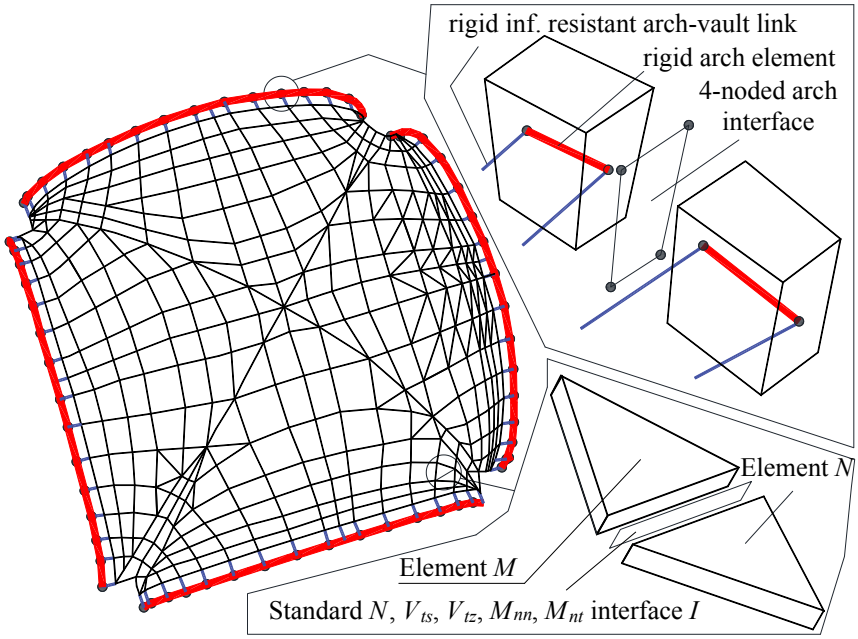

Figure 12: Details of the inelastic interfaces in the RBS approach

In this framework, the procedure here proposed belongs to a classic discretization procedure where Rigid Bodies are interconnected by equivalent Springs exhibiting an elasto-plastic behavior with softening (RBS Model).

Being the elements rigid, elastic and inelastic deformation results therefore lumped only on triangle/triangle, triangle/beam or beam/beam interfaces, where non-linear rotational and

translational equivalent springs are located. In RBSMs, the computational effort needed to perform non-linear static (and dynamic) analyses) is much less than in standard FEs and this is the reason why it is also adopted in this case study. The identification of springs stiffness is classic and occurs equating the elastic energy stored in the RBS system with that of the continuum, as discussed in detail in [67].

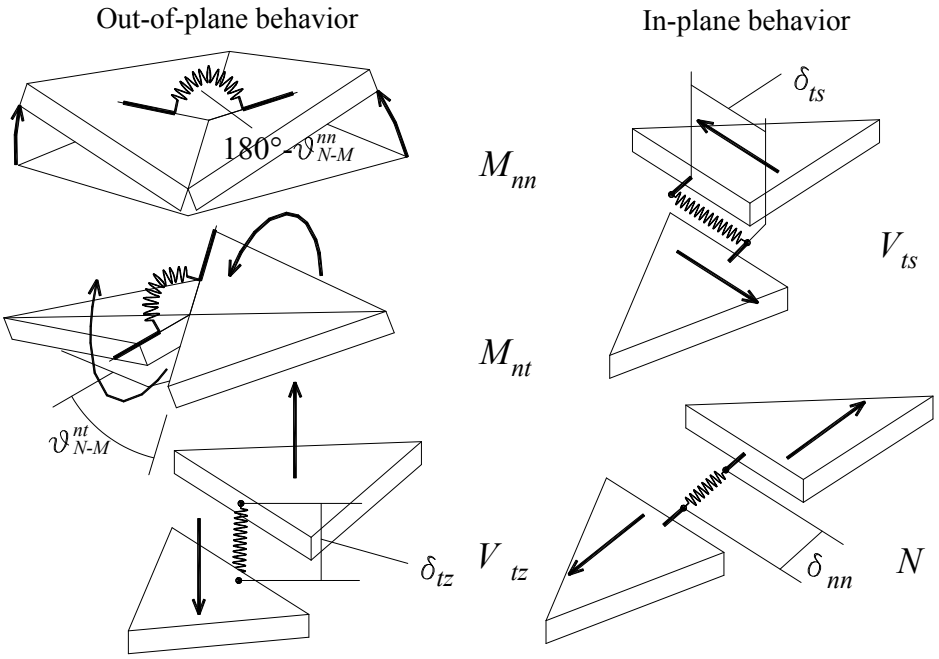

Figure 13: Details of the inelastic interfaces in the RBS approach

Two contiguous rigid elements with a common edge Γ_{12} (length equal to L_{12}) are considered. They are thought as interconnected in correspondence of the centroid by two shear springs, one axial spring, one flexural spring and one torsional spring, as depicted schematically in Figure 12.

Langrangian variables of a rigid element M are centroid displacements (u_x^M and u_y^M) and rotation Φ_z^M around centroid, all collected into vector $\mathbf{U}_M^T=[\,u_x^M\,;\,u_y^M\,;\,\Phi_z^M\,]$.

Displacement field of points on the edge Γ_{12} are provided by the following trivial formula:

$$\begin{bmatrix} u_{x0} \\ u_{y0} \end{bmatrix} = \begin{bmatrix} 1 & 0 & -(y_0 - y_M) \\ 0 & 1 & (x_0 - x_M) \end{bmatrix} \begin{bmatrix} u_x^M \\ u_y^M \\ \Phi_z^M \end{bmatrix} = \mathbf{R}_M(\mathbf{P}_0)\mathbf{U}_M \qquad (1)$$

Where x_0 and y_0 are the coordinates of $\mathbf{P}_0$ point on Γ_{12} edge and u_{x0} (u_{y0}) is the horizontal (vertical) displacement of the point.

Indicating with $\mathbf{s}^e$ ($\mathbf{r}^e$) the unitary vector parallel (perpendicular) to Γ_{12}, the transformation matrix from the global to the interface local coordinate system is:

$$\begin{bmatrix} \mathbf{s}^e \\ \mathbf{r}^e \end{bmatrix} = \begin{bmatrix} \mathbf{s}^e \bullet \mathbf{e}_1 & \mathbf{s}^e \bullet \mathbf{e}_2 \\ \mathbf{r}^e \bullet \mathbf{e}_1 & \mathbf{r}^e \bullet \mathbf{e}_2 \end{bmatrix} \begin{bmatrix} \mathbf{e}_1 \\ \mathbf{e}_2 \end{bmatrix} = \mathbf{T} \begin{bmatrix} \mathbf{e}_1 \\ \mathbf{e}_2 \end{bmatrix} \Leftrightarrow \begin{bmatrix} \mathbf{e}_1 \\ \mathbf{e}_2 \end{bmatrix} = \mathbf{T}^{-1} \begin{bmatrix} \mathbf{s}^e \\ \mathbf{r}^e \end{bmatrix} \quad (2)$$

where the symbol $\bullet$ indicates the internal product.

The jump of displacements on the interface Γ_{12} between M and N turns out therefore to be:

$$[\mathbf{u}^{M-N}] = \begin{bmatrix} \Delta u_n \\ \Delta u_t \end{bmatrix} = \mathbf{T}^{-1} \left[\mathbf{R}_M(\mathbf{P}_0)\mathbf{U}_M - \mathbf{R}_N(\mathbf{P}_0)\mathbf{U}_N \right] \quad (3)$$

where Δu^r and Δu^s are the normal and tangential jumps of displacement on the interface, respectively.

Joints on arches are assumed constituted by mortar, hence –where possible- with the same mechanical properties deduced experimentally.

Conversely, for the vault (which is constituted by very irregular stones) a homogenized material with isotropic behavior is assumed. Uniaxial stress-strain relationships assumed are summarized in Figure 14.

The assemblage of springs and rigid elements results into a standard multi-DOF model, or better an assemblage of mono-dimensional elements (non-linear springs) and masses (rigid elements) particularly simple to handle both in the non-linear static and non-linear dynamic range, exhibiting a promising robustness that a classic FE refined discretization with damaging materials cannot have.

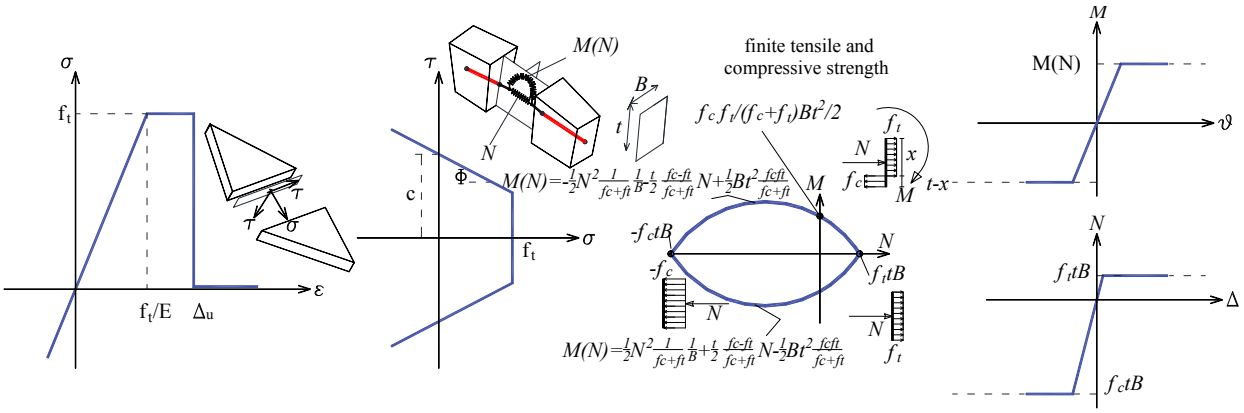

Figure 14: Left: Uniaxial stress strain relationship and frictional behavior assumed for triangle/triangle interfaces (vault). Right: beam/beam interfaces (perimeter walls) with bending moment and axial load relationships.

3.3 NURBS Kinematic Limit Analysis model (NURBS-KLA)

Recently, one of the authors has proposed in [48] a straightforward and effective limit analysis approach for the evaluation of collapse loads and failure mechanisms in masonry vaults with complex geometries, eventually in presence of FRP reinforcement (see [21] for details). Such approach bases on a rough discretization with Non Uniform Rational Beta Spline NURBS surfaces, assumed rigid infinitely resistant, where dissipation is allowed exclusively at the interfaces between contiguous

elements. Few NURBS elements allow to precisely reproduce curved shapes with complex geometries, but the utilization of a rough discretization combined with the restriction of dissipation allowed only on element edges is potentially responsible for a large overestimation of the collapse loads and an identification of incorrect failure mechanisms. In order to cope with such issue, a progressive adaptation of the mesh to match the actual failure mechanism has been hence embedded in the model presented in [48] and here used to analyze St John's vaults in the framework of limit analysis. The model adopted is depicted in Figure 15 and the only simplification assumed was to adapt the edge arches to a uniform thickness (an average between the two different edge lengths of the stones). The major advantage of such procedure relies indeed into the adoption of few NURBS elements; the utilization of one element per stone would go in the opposite direction, i.e. towards an analysis at fixed interfaces, locked into a heterogeneous approach for the arches and hence very inefficient in the procedure of the mesh adaptation. Furthermore, experimental tests to characterize block/mortar interfaces have shown how the hypothesis of no-tension material is here very suitable. There is therefore only the need to establish that the thrust-line remains completely inside the thickness of the arch, following the classic approach recommended by Heyman [9,28,68,69].

As far as the mechanical characterization of the interfaces is concerned, where possible experimental evidences have been adopted. Thanks to the very fast mesh adaptation procedure embedded in the limit analysis numerical model, full sensitivity analysis can be repeated changing the resultant masonry tensile strength.

For perimeter arches, as already discussed, a no-tension material model is assumed, with no possibility of sliding one element-element interfaces. In other words, it is made the hypothesis of formation of flexural hinges only. Such assumptions are in agreement with both Heyman's hypotheses on arches (which proved to be effective in almost the totality of the cases) and the actual behavior of the experimented vaults.

For irregular masonry belonging to the vault, a very low tensile strength equal to 0.01 MPa and corresponding to the experimental value of the resistance at the block/mortar interfaces determined experimentally via direct tensile tests (see previous Section) is assumed.

Particular attention deserves the determination of the interfaces tangential behavior. As a matter of fact, it was not possible to characterize under shear the typology of masonry used to build the vault, but what emerges from the technical literature for sandstone with cement-lime mortar is a reasonably high friction angle (30°), which numerically allows a formation of a failure mechanism characterized by a mutual roto-translations of contiguous blocks at the interfaces, without premature loss of equilibrium due to pure sliding.

Compressive strength of the masonry material is assumed infinite, again in agreement with both experimental data and consolidated literature for vaults.

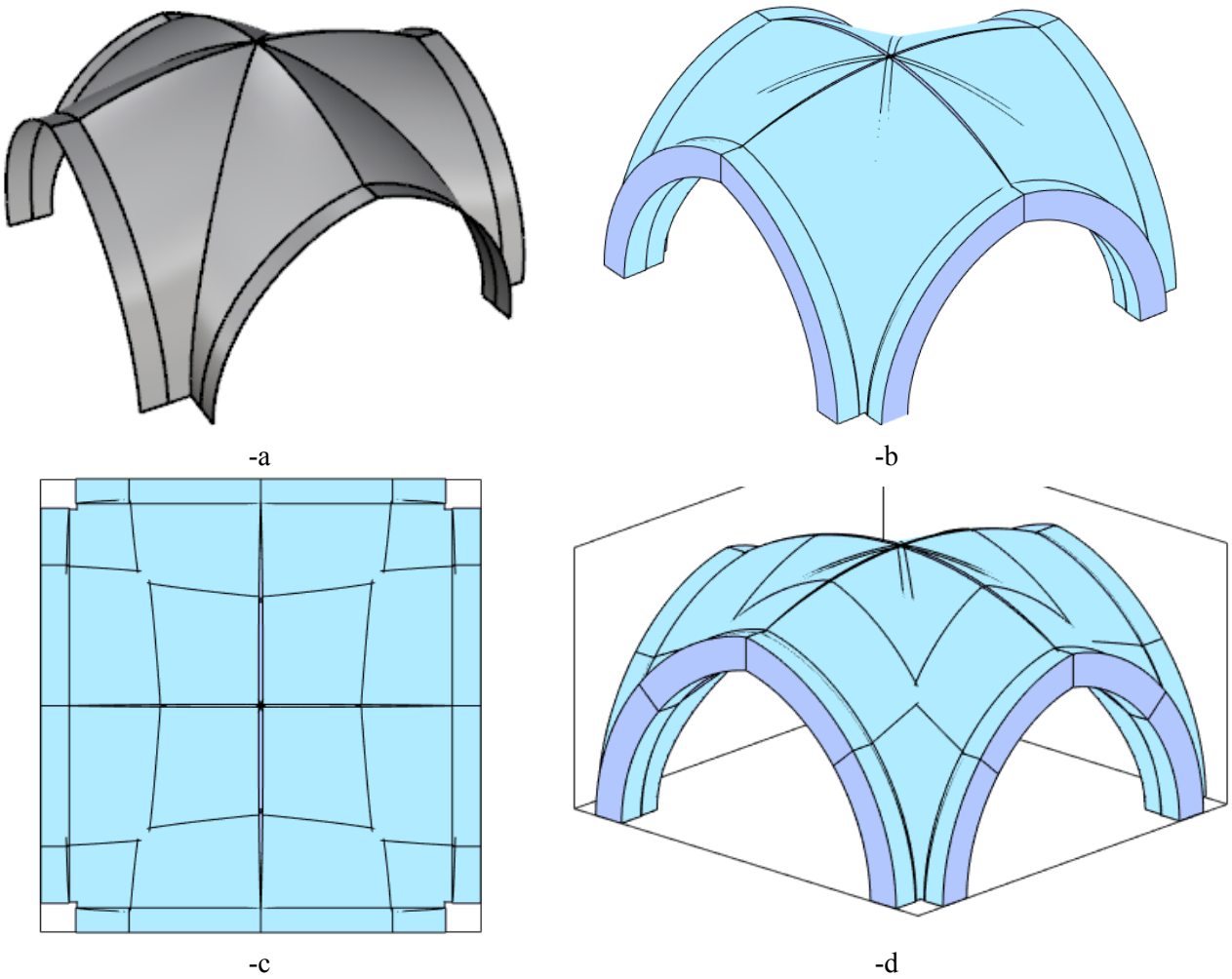

Figure 15. NURBS model in Rhinoceros® (-a) and imported in MATLAB® (-b) where limit analyses are carried out. –c & -d: plane and perspective view of the initial mesh utilized.

3.4 Discretization used

A quite refined FE discretization is adopted to analyze numerically the vaults using both the CDP and the RBS approaches, as depicted in Figure 16-a and -b. In particular, a 3D model constituted by 21122 nodes and 97926 tetrahedron elements is utilized, with at least 4 elements along the thickness to properly account for the inelastic flexural behavior of the vault. As far as perimeter arches are concerned, a heterogeneous approach with elastic blocks and cohesive-friction interfaces representing joints would be the most suitable, but at the same time authors experienced a further worsening of the numerical effort needed to perform computation and a progressive deterioration of the stability of the arc-length algorithm. To justify the utilization of an isotropic material without interfaces for arches, two main issues are worth noting: (1) classically arches are studied at failure as made by a homogeneous material with little or no tensile resistance and plotting the line of thrust (i.e. assuming that failure is possible only in bending) and (2) results obtained with the second procedure presented

in this paper (see after), where a heterogeneous model is adopted for arches, do not differ significantly from the outcome obtained with CDP model.

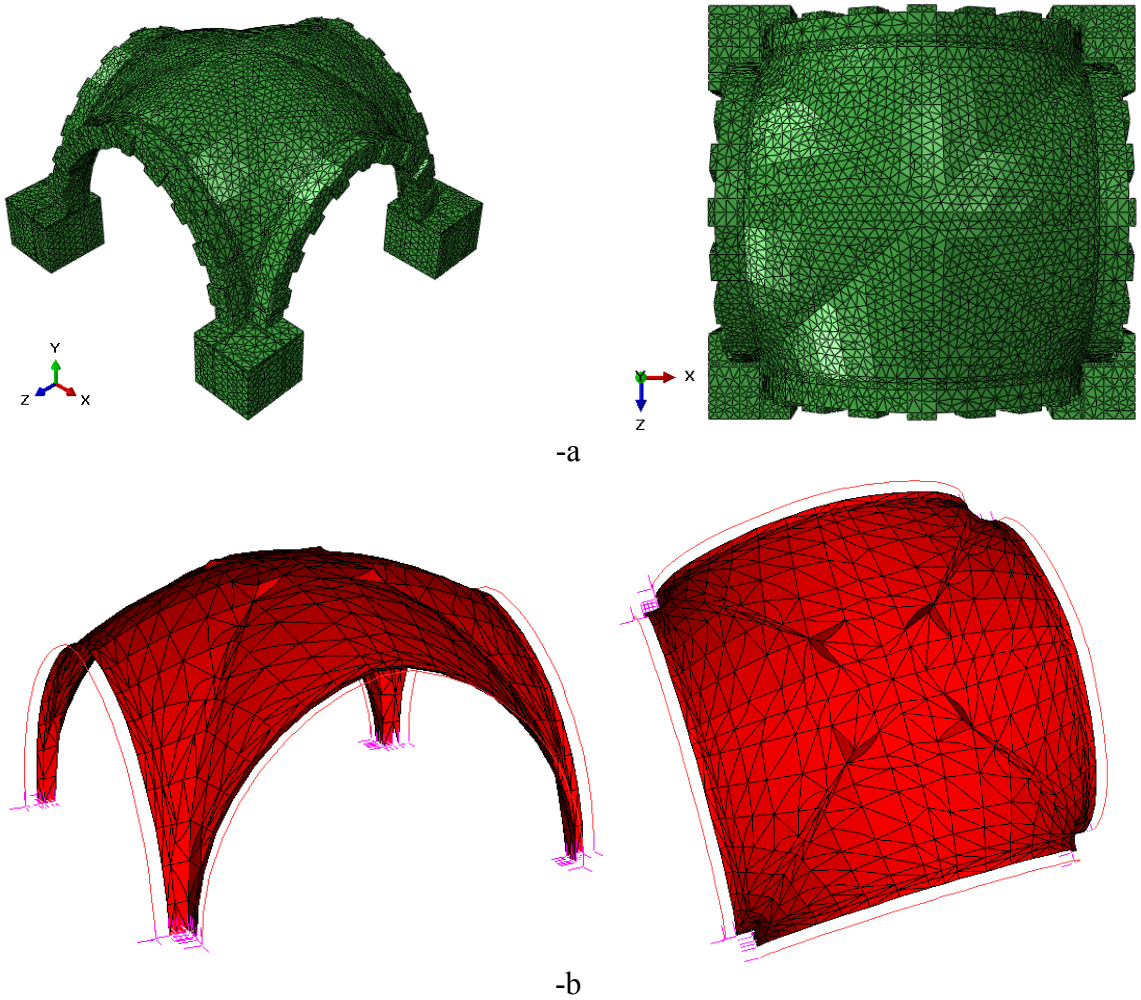

Figure 16: FE discretization adopted to perform numerical simulations in (-a) Abaqus and with the SQP approach (-b).

3.5 FRP reinforcement modelling

The strengthened vault is obtained applying at the extrados of the repaired vault a system of FRP strips in correspondence of the edges and on diagonal arches. From a numerical point of view, to account for the FRP strengthening, a consolidated approach already adopted in e.g. [16] and suggested by the Italian code on innovative reinforcement for r.c. and masonry structures (CNRDT200 [53]) is adopted.

The approach relies into the utilization for FRP strips of equivalent truss elements perfectly bonded to the support with elasto-fragile behavior in tension and unable to resist in compression (in order to take into account buckling due to the particularly thin cross section).

The assumption of a perfect bond between masonry and FRP layers deserves additional comments. As a matter of fact, such hypothesis a priori excludes any possibility of delamination, an important issue for FRP reinforcement on fragile materials as masonry.

In fact, when delamination from the support occurs, the effectiveness of FRP reinforcement vanishes. This phenomenon is very complex to model, because it involves materials with different properties (masonry, FRP and glue layer) and depends on several parameters. Experimental studies [53] demonstrated that the decohesion occurs because of the failure of the masonry material; in fact, the delaminated FRP presents a consistent layer of masonry material on the debonded surface.

Several authors, not only for FRP but also for FRCM and TRM see e.g. [68,69,70-78]**,** utilize interface elements interposed between masonry and FRP reinforcement, but this is quite cumbersome numerically and requires the knowledge of FRP/masonry interface mechanical properties, i.e. a set of parameters difficult to characterize experimentally. In other cases, simplified approaches based on a discretization with springs is preferred [80–83], which appears a good compromise between complexity and numerical efficiency.

Italian Guidelines CNR-DT200 in their revised version R1 [53] allow to use perfectly bonded elements with fictitious tensile strength, accounting for delamination through the design fracture energy Γ_{Fd} of the FRP-substrate interface.

Such interface exhibits a tangential stress-slip bilinear behavior (elastic-with linear softening), characterized by a ultimate slip s_u and a peak tangential strength $f_{bd} = 2\Gamma_{Fd} / s_u$. Fracture energy Γ_{Fd} is defined as follows:

$$\Gamma_{Fd} = \frac{k_b k_G}{FC}\sqrt{f_{bm} \cdot f_{btm}} \quad [f \text{ in } N/mm^2] \tag{4}$$

where:

- k_b is a geometric correction coefficient that, in the absence of experimental data, is equal to $\sqrt{\frac{3-b_f/b}{1+b_f/b}}$, being b the width of the structural element to reinforce and b_f the reinforcement width. b is typically assumed equal to the dimension of the brick perpendicular to the reinforcement axis.

- k_G is a further correction coefficient derived from the results of experimental tests, expressed in mm and dependent on the masonry type. In the case of in-situ impregnated reinforcements and for masonry, k_G *=0.031 mm.*

- FC is the so called confidence factor, which is related to the knowledge level LC according to Table C8A.1.1 of the Italian code. There are three LCs, from 1 to 3, related to the level of knowledge about the mechanical and geometrical properties of the structure: LC3 is the maximum, whereas LC1 is the

minimum one. Since the comparison is done with respect to the laboratory in-scale model, LC3 is assumed.

- f_{bm} is the average compressive strength of the blocks;

- f_{btm} is the average tensile strength of the blocks.

Fracture energy is used by the Italian Guidelines CNR-DT200 also to model –as done here- a perfect bond between layers with reduced axial strength of the fibers (modelled as trusses), to properly account for the possible delamination. Two different failure modes are hypothesized, the first (mode 1) consists on a detachment at the ends of the strip, whereas the second (failure mode 2) is a detachment in the middle of the strip. In any case, the evaluated FRP peak strength should not exceed the design bond strength f_{fdd} given for mode 1 by the following equation:

$$f_{fdd} = \frac{1}{\gamma_{f,d}} \sqrt{\frac{2 \cdot E_f \cdot \Gamma_{fd}}{t_f}} \qquad (5)$$

where the symbols have the following meanings:

- $f_{fdd,rid}$ is the reduced value of the design bond strength;
- f_{fdd} is the design bond strength;
- E_f is the Young modulus of FRP reinforcement;
- t_f represents the FRP thickness;
- $\gamma_{f,d}$ is a factor taking into account the modality of the FRP reinforcement system application and assumed ranging between 1.2 and 1.5;

When the anchorage length l_b is smaller than the optimal bond length l_{ed} a reduction of the design bond strength is introduced as follows:

$$f_{fdd,rid} = f_{fdd} \frac{l_b}{l_{ed}} \left(2 - \frac{l_b}{l_{ed}} \right) \qquad (6)$$

Where the optimal bond length is evaluated as follows:

$$l_{ed} = \max \left\{ \frac{1}{\gamma_{Rd} f_{bd}} \sqrt{\frac{\pi^2 E_f t_f \Gamma_{Fd}}{2}}; 150mm \right\} \qquad (7)$$

where:

- f_{bd} is the brick design compressive strength
- γ_{Rd} is a factor equal to 1 for bending, 1.2 for shear and 1.1 for columns hooping.

For failure mode 2, the design bond strength $f_{dd,2}$ is:

$$f_{dd,2} = \frac{k_q}{\gamma_{f,d}} \sqrt{\frac{E_f 2\, k_b\, k_{G,2}}{t_f \quad FC}} \sqrt{f_{bm} f_{btm}} \qquad (8)$$

where:

- k_q is a coefficient that takes into account the load conditions: it is equal to 1.25 for predominant distributed loads and equal to 1 in all the other cases.
- $k_{G,2}$ is a correction coefficient derived from experimental test results: it is equal to 0.1 mm.

According to the aforementioned indications, mechanical properties adopted for the equivalent FRP trusses are provided in Table 6.

Table 6: Mechanical properties adopted for equivalent FRP trusses

E_{FRP} [MPa]	193000
Γ_{FK} [N/mm]	0.013
$f_{f\,dd}$ [MPa]	116.4

4 Numerical results

In this Section, the numerical results obtained analyzing the vault, before in absence of reinforcement and then in presence of FRP strengthening) by means of the three numerical approaches proposed (FE-CDP, RBS and NURBS-KLA respectively) are presented and critically discussed and a deep insight into the expected seismic behavior is obtained.

4.1 Unreinforced vault

Figure 17 depicts force displacement curves obtained with CDP and RBS models, compared with experimental data, in case of the vault without reinforcement. In Figure 17, x axis is represented by the horizontal displacement of the keystone of the perimeter arch CD, i.e. DT04 (juxtaposed to the application point of the concentrated load), but authors experienced a similar behavior DT01. It is interesting to notice the good agreement between numerical models predictions (especially elastic stiffness and ultimate load carrying capacity) and experimental evidences.

In the case of the FE-CDP model, which is an approach where damage of the material is present, it is also possible to evaluate its global fitting capabilities under loading unloading cycles. In contrast, for RBS model, which is elasto-plastic, the unloading phase occurs always with the slope of the virgin material and therefore it results intrinsically unsuited for an utilization under cyclic loads and non-linear dynamic problems.

As can be noted from Figure 17, CDP results slightly stiffer than experimental data in the three unloading phases done experimentally, even if the behavior can be still considered satisfactory from practical purposes. Such a result can be a consequence of a suboptimal selection of damage and elasto-plastic parameters, which together rule the unloading phase. Authors are aware that a further effort in

refining the numerical values adopted for CDP would have improved further the fitting in the unloading phase (which is still considered acceptable), being however such tuning not the object of the present computations.

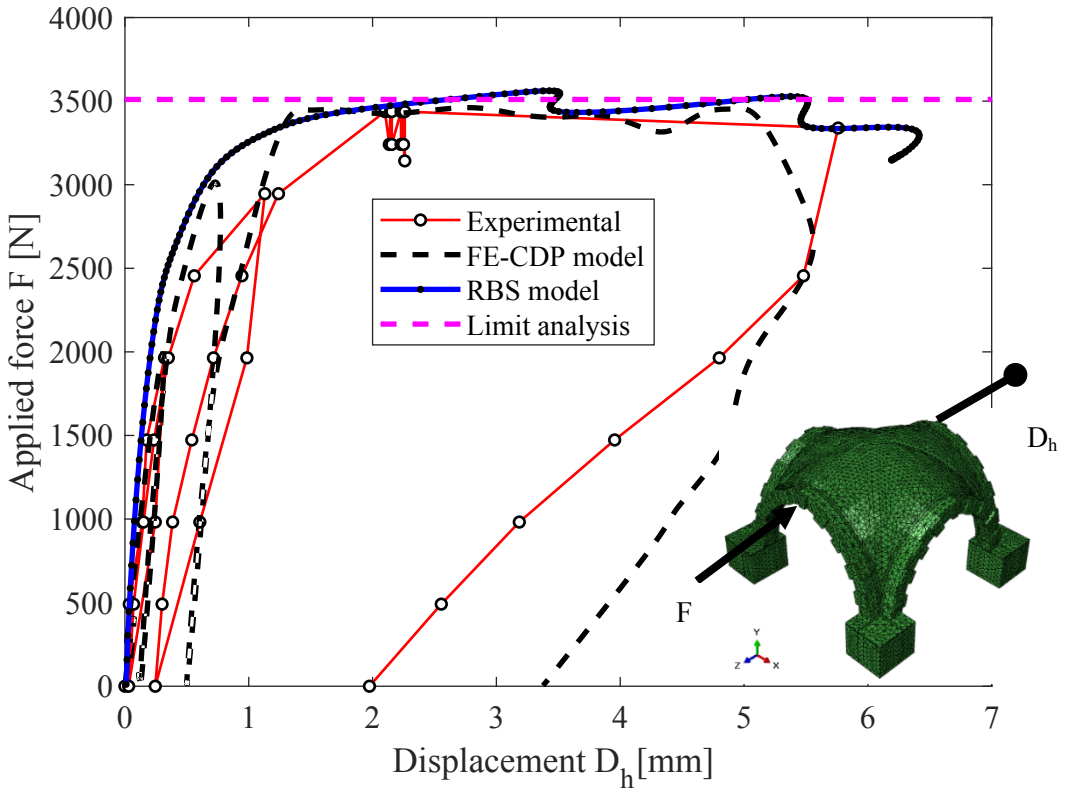

Figure 17: Unreinforced vault. Global force F-displacement D_h (DT4) obtained numerically and comparison with experimental data.

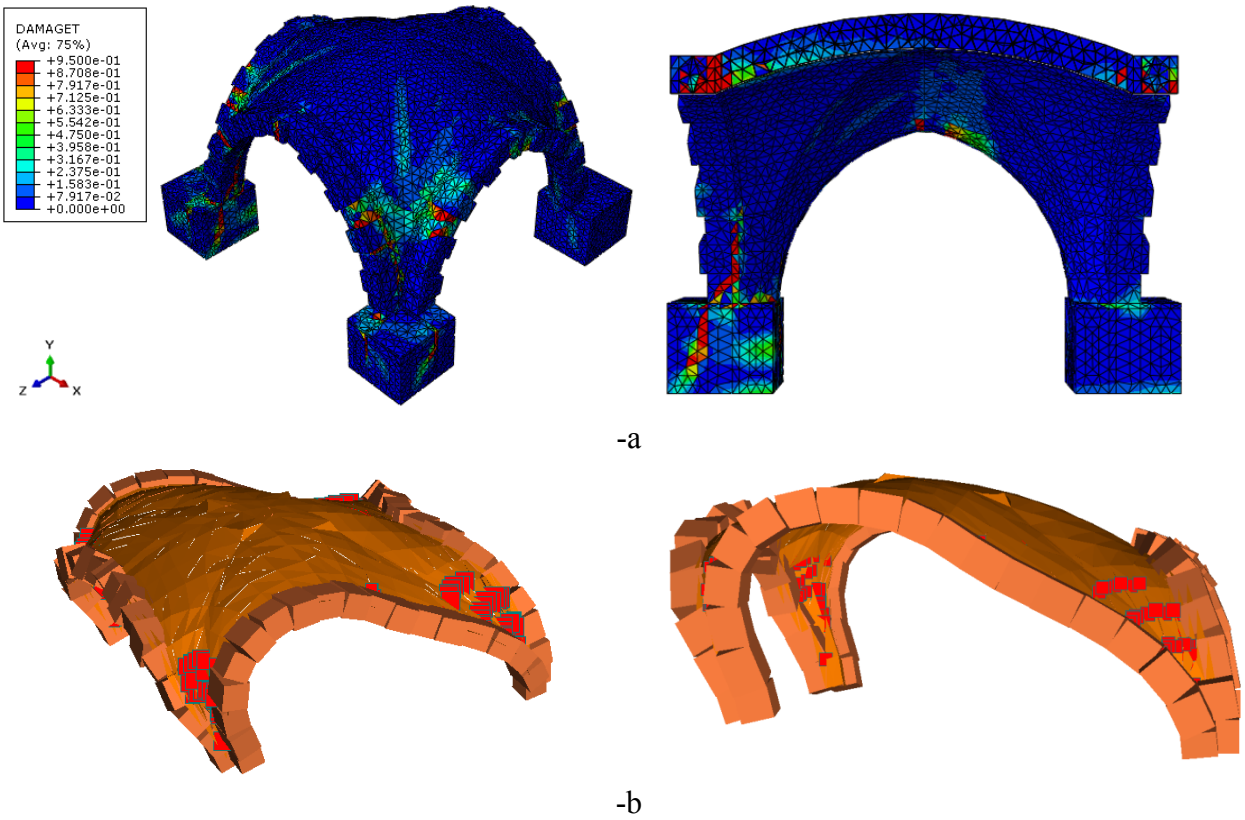

Figure 18: Unreinforced vault. -a: tensile damage color patch at failure for FE-CDP model. –b: deformed shape at collapse and indication of cracked interfaces for the RBS model.

In Figure 19 the failure mechanism found using NURBS-KLA code (after mesh adaptation) is shown using two different perspective views. As can be noted, the lateral arches parallel to the direction of the load form three clear flexural hinges, Especially two, that at one fourth of the span and the other in the middle span are in almost perfect agreement with both CDP and RBS models, see Figure 18. The lunette-shape cracks arising in the vault at one fourth are again in very good agreement with alternative numerical approaches and experimental outcome. The resultant load carrying capacity with a tensile strength equal to the experimental one (0.01 MPa) is about 3.5kN, Figure 20, again in excellent agreement with both alternative computationally expensive numerical approaches and experimental results.

The sensitivity analysis reported in Figure 20 is carried out varying masonry vault tensile strength and assuming two different cohesion c values to represent the tangential behavior of the dissipating interfaces, namely equal respectively to f_t (i.e. almost vanishing) and 0.3 MPa. The second case, with very large cohesion locks the interfaces to fail exclusively for normal/flexural actions, whereas any sliding is in practice precluded. Such assumption results into an obvious overestimation of the collapse load, with an associated active mechanism purely ruled by the flexural behavior. The difference when compared with results obtained with assumptions on the mechanical properties of

masonry that are more realistic and close to experimental ones is visible mainly in terms of collapse loads, as expected, but not perceivable on the collapse mechanisms associated. It is therefore reasonable to conclude that sliding has a secondary effect in the definition of a clear crack patterns; in other words, sliding occurs and tends to decrease the load carrying capacity, but the mechanism is dominated by bending. Such outcome is important in the correct design of a possible strengthening system aimed at reducing the seismic vulnerability, as it will be discussed in the following Sections, more that in a reliable evaluation of the load carrying capacity.

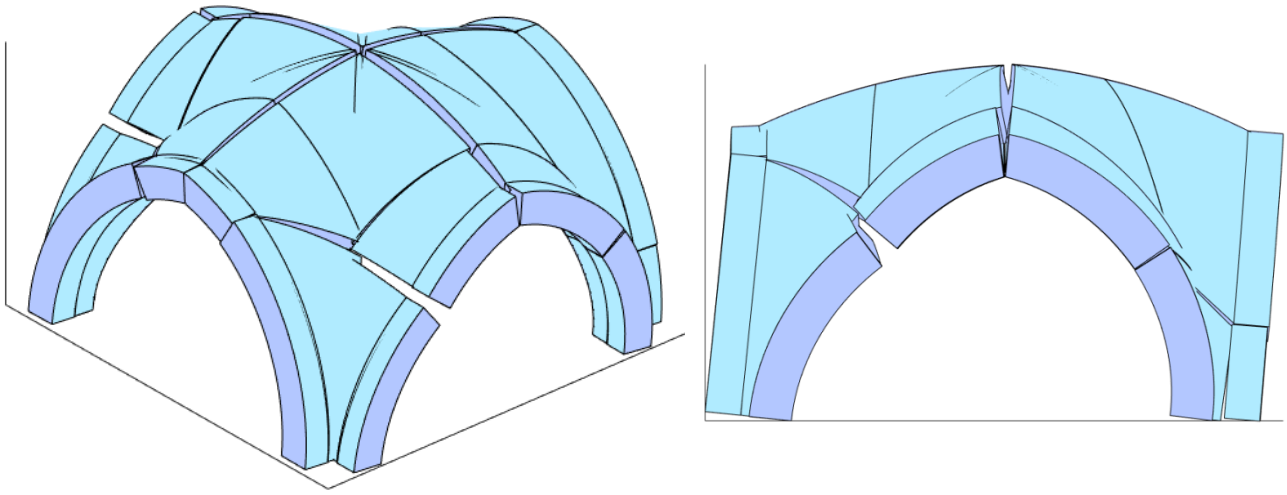

-a -b

Figure 19: Collapse mechanism for the unreinforced vault. Perspective (–a) and (-b) lateral views.

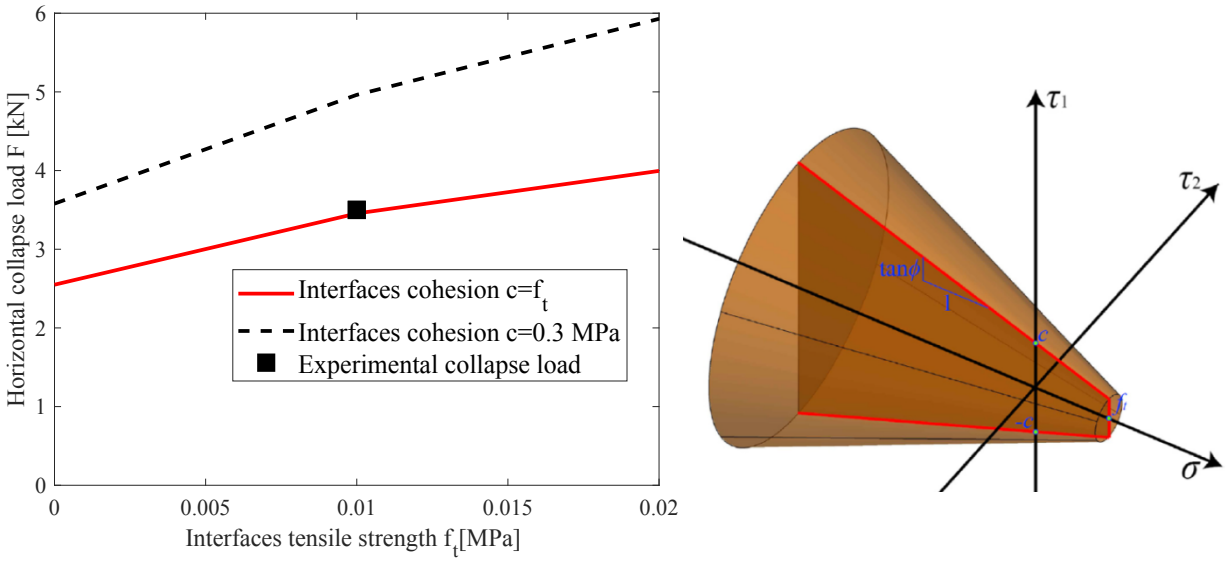

Figure 20: Sensitivity analysis (left) on the unreinforced vault collapse load varying vault tensile strength and strength domain assumed for the interfaces (right).

4.2 FRP reinforced vault

The reinforced vault is numerically analyzed taking into account the actual state of damage obtained in the unreinforced case, because the vault was reinforced without repairing the cracks with injections. In the FE CDP model, it was possible to export the state of damage exhibited by the model in the last step of analysis of the unreinforced case and subsequently re-import in the initial step of the analysis with the reinforcement (as "predefined field" in the Abaqus environment). A similar procedure was adopted in the RBS model, assuming in this latter case stress-strain relationships of the damaged interfaces different from those resulting undamaged in the unreinforced case.

Global load-displacement curves of the loaded key-stone (analogously to what done for the unreinforced case) are shown in Figure 21. As can be observed, both models (FE-CDP and RBS) fit almost perfectly the experimental data. As far as the final unloading phase for FE-CDP is concerned, it should be pointed out that, similarly to the unreinforced case, a stiffer behavior is exhibited by the numerical model, indicating once again that a slight improvement of the tuning procedure for damage parameters and plastic strains would be needed. In this case, failure mechanism is characterized by a quite visible horizontal sliding of the entire vault (as quasi-rigid body) over horizontal cracks located near the base supports. Such a rigid translation of the whole vault is obviously a consequence of the strong reinforcement placed at the extrados, which basically does not allow the formation of flexural cracks at the extrados of both the vault and the edge arches. Crack patterns and deformed shapes at collapse found with both models, see Figure 22, confirm the experimental behavior of the structure. The softening behavior exhibited globally by the vault is due to a detachment of the reinforcement near the supports.

Limit analysis computations are carried out on the adjusted mesh found at the last iteration in the unreinforced case, see Figure 19, but where new adapting interfaces are utilized, already cracked interfaces forming the failure mechanism are assumed freezed and unable to resist tensile stresses. FRP strips are added as rigid-perfectly plastic truss elements with equivalent strength as in Eqs. (5)(8).

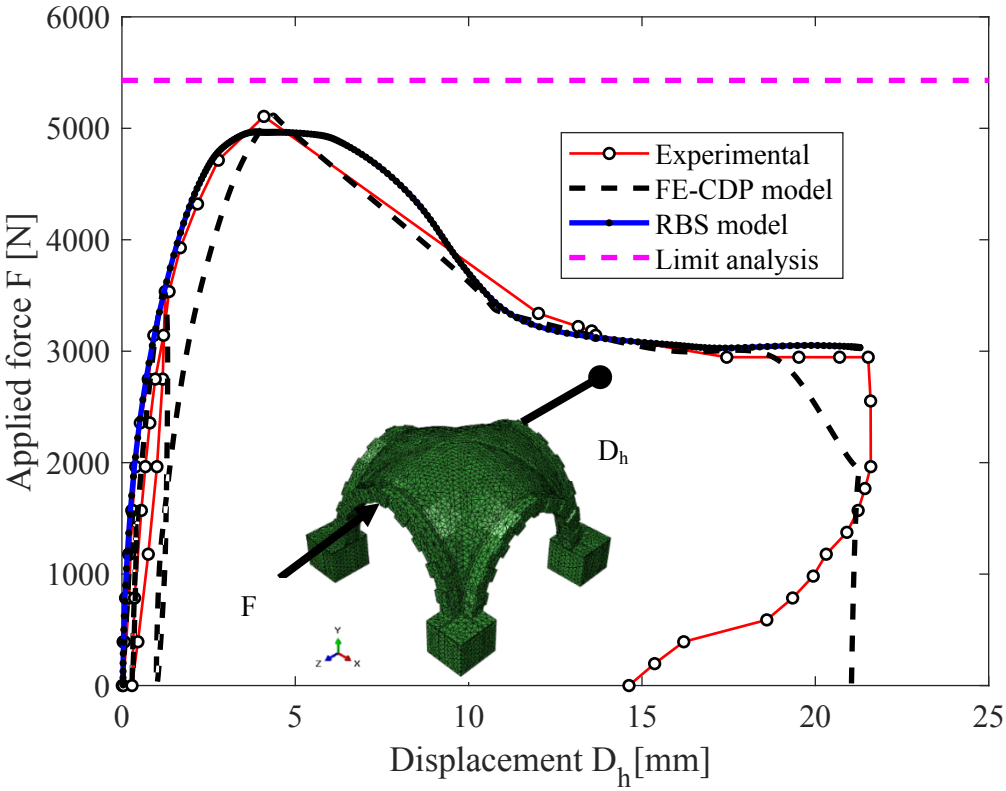

Figure 21: FRP-reinforced vault. Global force F-displacement D_h (DT4) obtained numerically and comparison with experimental data.

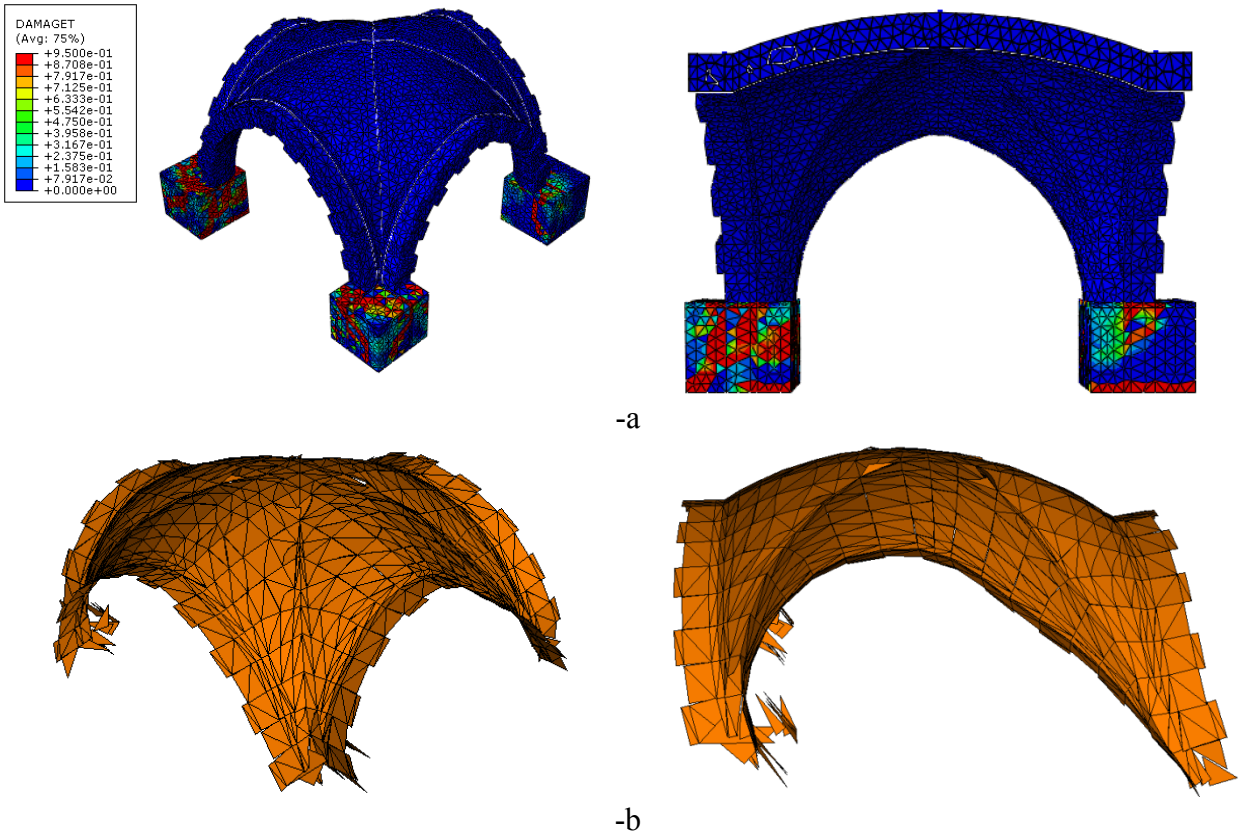

-a

-b

Figure 22: FRP-reinforced vault. -a: tensile damage color patch at failure for FE-CDP model. –b: deformed shape at collapse for RBS model.

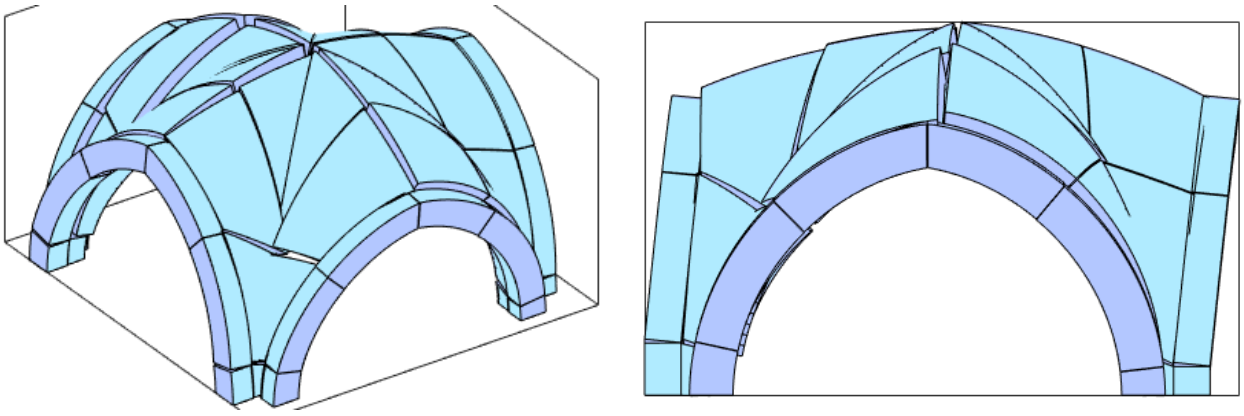

-a -b

Figure 23: Collapse mechanism for the FRP-reinforced vault found with adaptive NURBS limit analysis. (a) perspective and (b) lateral views.

5 Conclusions

Three advanced non-linear modelling strategies for the evaluation of the load carrying capacity under horizontal loads of an historical groin vault in Jerusalem of major importance have been presented. The first model is a concrete damage plasticity macroscopic approach implemented in Abaqus where masonry is assumed elasto-plastic with damage in both tension and compression and scarcely resistant to tensile stresses. The second is a non commercial Rigid Body and Spring Model approach, where the structure is discretized into rigid elements and elasto-plastic with softening interfaces. Arches are modeled with a heterogeneous approach, whereas the vault through an elasto-plastic isotropic material with quasi zero tensile strength and softening behavior. The last model is an upper bound limit analysis with adaptive mesh, where NURBS elements are utilized.

For validation purposes, an in-scale 1:5 model of the groin vault has been tested at the University of Florence under horizontal loads up to collapse, also in presence of FRP reinforcement. The experimental tests carried out on the unreinforced and FRP reinforced scale model have shown rather similar qualitative results, which on the contrary differ in quantitative terms. The first load cycles show an almost linear elastic behavior up to 57% and 68% of the peak load in the unreinforced and reinforced model, respectively equal to 3.50 kN and 5.10 kN. After the peak load has been achieved, the vertical displacements increase with an almost constant load, meaning that failure mechanisms have already occurred. Moreover, since the beginning, the vertical displacements of the keystones have opposite sign, clearly indicating a rotation of the vault around a horizontal axis, orthogonal to the load direction. The cracks in the unreinforced model occur mainly in correspondence of the springers of the vault, whereas in the reinforced model they are mostly vertical, probably due to a greater crushing, and concentrated on the pillars, so highlighting a monolithic behavior of the strengthened vault.

The numerical results obtained on the unreinforced model by means of the proposed numerical approaches (FE-CDP, RBS and NURBS kinematic limit analysis) show a clear coincidence with the experimental results. In particular, it is possible to note a good agreement between numerical simulations and the experimental evidences in terms of elastic stiffness (when present in the model, i.e. outside limit analysis), ultimate load carrying capacity and active failure mechanisms. It is worth noting that the comparison with the experimental results also allows to evaluate the different global fitting capabilities of FE-CDP under loading-unloading cycles.

The analyses carried out with the same numerical approaches on the reinforced model show again an excellent agreement in terms of horizontal displacements measured at the key stones in the direction of the applied horizontal load. The beneficial effects of the FRP are clearly visible, especially in the change in the failure mechanism, an insight which can be straightforwardly provided by limit analysis. FE-CDP and RBS, on the other hand, show how the key stones of the arches orthogonal to the load direction have vertical displacements only in the range 1-3 mm, which denote a greater stiffness of the arches. Still in agreement with the experimental results all cracks occur inside the un reinforced pillars, whereas vault and lateral arches remain not damaged.

6 References

[1] Tralli A, Alessandri C, Milani G. Computational methods for masonry vaults: A review of recent results. Open Civ Eng J 2014;8:272–87. doi:10.2174/1874149501408010272.

[2] Gaetani A, Lourenço PB, Monti G, Milani G. A parametric investigation on the seismic capacity of masonry cross vaults. Eng Struct 2017;148:686–703. doi:10.1016/j.engstruct.2017.07.013.

[3] Fraternali F. A thrust network approach to the equilibrium problem of unreinforced masonry vaults via polyhedral stress functions. Mech Res Commun 2010;37:198–204. doi:10.1016/j.mechrescom.2009.12.010.

[4] Foti D, Vacca V, Facchini I. DEM modeling and experimental analysis of the static behavior of a dry-joints masonry cross vaults. Constr Build Mater 2018;170:111–20. doi:10.1016/j.conbuildmat.2018.02.202.

[5] Rossi M, Calderini C, Lagomarsino S. Experimental testing of the seismic in-plane displacement capacity of masonry cross vaults through a scale model. Bull Earthq Eng 2016;14:261–81. doi:10.1007/s10518-015-9815-1.

[6] Milani G, Valente M, Alessandri C. The narthex of the Church of the Nativity in Bethlehem: A non-linear finite element approach to predict the structural damage. Comput Struct 2018;207:3–18. doi:10.1016/j.compstruc.2017.03.010.

[7] Gaetani A, Monti G, Lourenço PB, Marcari G. Design and Analysis of Cross Vaults Along History. Int J Archit Herit 2016;10:841–56. doi:10.1080/15583058.2015.1132020.

[8] Bertolesi E, Adam JM, Rinaudo P, Calderón PA. Research and practice on masonry cross vaults – A review. Eng Struct 2019;180:67–88. doi:10.1016/j.engstruct.2018.10.085.

[9] Huerta S. The debate about the structural behaviour of gothic vaults: From violletle-duc to heyman. Proc Third Int Congr Constr Hist 2009:837–44.

[10] Lengyel G, Bagi K. Numerical analysis of the mechanical role of the ribs in groin vaults. Comput Struct 2015;158:42–60. doi:10.1016/j.compstruc.2015.05.032.

[11] Theodossopoulos D, Sinha BP, Usmani AS, Macdonald AJ. Assessment of the structural response of masonry cross vaults. Strain 2002;38:119–27. doi:10.1046/j.0039-2103.2002.00021.x.

[12] Lengyel G. Discrete element analysis of gothic masonry vaults for self-weight and horizontal support displacement. Eng Struct 2017;148:195–209. doi:10.1016/j.engstruct.2017.06.014.

[13] Creazza G, Matteazzi R, Saetta A, Vitaliani R. Analyses of masonry vaults: A macro approach based on three-dimensional damage model. J Struct Eng 2002;128:646–54. doi:10.1061/(ASCE)0733-9445(2002)128:5(646).

[14] Coccia S, Como M. Minimum thrust of rounded cross vaults. Int J Archit Herit 2015;9:468–84. doi:10.1080/15583058.2013.804965.

[15] Milani G, Lourenço PB, Tralli A. Homogenised limit analysis of masonry walls, Part II: Structural examples. Comput Struct 2006;84:181–95. doi:10.1016/j.compstruc.2005.09.004.

[16] Grande E, Milani G, Sacco E. Modelling and analysis of FRP-strengthened masonry panels. Eng Struct 2008;30:1842–60. doi:10.1016/j.engstruct.2007.12.007.

[17] Milani G, Shehu R, Valente M. A kinematic limit analysis approach for seismic retrofitting of masonry towers through steel tie-rods. Eng Struct 2018;160:212–28. doi:10.1016/j.engstruct.2018.01.033.

[18] Valente M, Milani G. Effects of Geometrical Features on the Seismic Response of Historical Masonry Towers. J Earthq Eng 2017:1–33. doi:10.1080/13632469.2016.1277438.

[19] Valente M, Milani G. Damage assessment and partial failure mechanisms activation of historical masonry churches under seismic actions: Three case studies in Mantua. Eng Fail Anal 2018;92:495–519. doi:10.1016/j.engfailanal.2018.06.017.

[20] Milani G, Milani E, Tralli A. Approximate limit analysis of full scale FRP-reinforced masonry buildings through a 3D homogenized FE package. Compos Struct 2010;92:918–35. doi:10.1016/j.compstruct.2009.09.037.

[21] Chiozzi A, Milani G, Tralli A. Fast kinematic limit analysis of FRP-reinforced masonry vaults. II: Numerical simulations. J Eng Mech 2017;143. doi:10.1061/(ASCE)EM.1943-7889.0001268.

[22] De Lorenzis L, Dimitri R, La Tegola A. Reduction of the lateral thrust of masonry arches and vaults with FRP composites. Constr Build Mater 2007;21:1415–30. doi:10.1016/j.conbuildmat.2006.07.009.

[23] Szołomicki J, Berkowski P, Barański J. Computer modelling of masonry cross vaults strengthened with fiber reinforced polymer strips. Arch Civ Mech Eng 2015;15:751–66. doi:10.1016/j.acme.2014.05.006.

[24] Fraternali F, Carpentieri G, Modano M, Fabbrocino F, Skelton RE. A tensegrity approach to the optimal reinforcement of masonry domes and vaults through fiber-reinforced composite

materials. Compos Struct 2015;134:247–54. doi:10.1016/j.compstruct.2015.08.087.

[25] Safeguarding the cultural heritage of Jerusalem – UNESCO resolution – Question of Palestine n.d. https://www.un.org/unispal/document/safeguarding-the-cultural-heritage-of-jerusalem-unesco-resolution-3/ (accessed December 13, 2018).

[26] Simulia DS. Abaqus 6.12 documentation. Provid Rhode Island, US 2012. doi:10.1097/TP.0b013e31822ca79b.

[27] Como M. Statics of Historic Masonry Constructions. Statics Hist Mason Constr 2013.

[28] Heyman J. The safety of masonry arches. Int J Mech Sci 1969;11:363–"382,IN3–IN4,383–385".

[29] Heyman J. Equilibrium of masonry arches. Proc Inst Civ Eng Eng Comput Mech 2010;163:129–33. doi:10.1680/eacm.2010.163.3.129.

[30] Bertolesi E, Milani G, Fedele R. Fast and reliable non-linear heterogeneous FE approach for the analysis of FRP-reinforced masonry arches. Compos Part B Eng 2016;88:189–200. doi:10.1016/j.compositesb.2015.11.005.

[31] Stockdale G, Tiberti S, Camilletti D, Sferrazza Papa G, Basshofi Habieb A, Bertolesi E, et al. Kinematic collapse load calculator: Circular arches. SoftwareX 2018;7:174–9. doi:10.1016/j.softx.2018.05.006.

[32] Carozzi FG, Poggi C, Bertolesi E, Milani G. Ancient masonry arches and vaults strengthened with TRM, SRG and FRP composites: Experimental evaluation. Compos Struct 2018;187:466–80. doi:10.1016/j.compstruct.2017.12.075.

[33] Bati SB, Fagone M, Rotunno T. Lower bound limit analysis of masonry arches with CFRP reinforcements: A numerical method. J Compos Constr 2013;17:543–53. doi:10.1061/(ASCE)CC.1943-5614.0000350.

[34] Galassi S. Analysis of masonry arches reinforced with FRP sheets: Experimental results and numerical evaluations. MATEC Web Conf., vol. 207, 2018. doi:10.1051/matecconf/201820701002.

[35] Bui TT, Limam A, Sarhosis V, Hjiaj M. Discrete element modelling of the in-plane and out-of-plane behaviour of dry-joint masonry wall constructions. Eng Struct 2017. doi:10.1016/j.engstruct.2017.01.020.

[36] Sarhosis V, Garrity SW, Sheng Y. Influence of brick-mortar interface on the mechanical behaviour of low bond strength masonry brickwork lintels. Eng Struct 2015. doi:10.1111/nph.14995.

[37] Sarhosis V, Garrity S, Sheng Y. Discrete Element Modeling of Masonry Wall Panels with Openings. 9th Intern. Conf. Comput. Struct. Technol., 2008. doi:10.4203/ccp.88.17.

[38] Kassotakis, Nicko and Sarhosis, Vasilis and Forgàcs, Tamàs and Bagi K. Discrete element modelling of multi-ring brickwork masonry arches. 13th Can. Mason. Simp., 2017.

[39] Lemos J V. Discrete element modeling of masonry structures. Int J Archit Herit 2007. doi:10.1080/15583050601176868.

[40] Azevedo J, Sincraian G, Lemos J V. Seismic behavior of blocky masonry structures. Earthq Spectra 2000. doi:10.1193/1.1586116.

[41] Çaktı E, Saygılı Ö, Lemos J V., Oliveira CS. Discrete element modeling of a scaled masonry structure and its validation. Eng Struct 2016. doi:10.1016/j.engstruct.2016.07.044.

[42] Casolo S, Milani G, Uva G, Alessandri C. Comparative seismic vulnerability analysis on ten masonry towers in the coastal Po Valley in Italy. Eng Struct 2013;49:465–90. doi:10.1016/j.engstruct.2012.11.033.

[43] Casolo S, Milani G. Simplified out-of-plane modelling of three-leaf masonry walls accounting for the material texture. Constr Build Mater 2013;40:330–51. doi:10.1016/j.conbuildmat.2012.09.090.

[44] Bertolesi E, Milani G, Casolo S. Homogenization towards a mechanistic Rigid Body and Spring Model (HRBSM) for the non-linear dynamic analysis of 3D masonry structures. Meccanica 2018;53:1819–55. doi:10.1007/s11012-017-0665-6.

[45] Chiozzi A, Grillanda N, Milani G, Tralli A. UB-ALMANAC: An adaptive limit analysis NURBS-based program for the automatic assessment of partial failure mechanisms in masonry churches. Eng Fail Anal 2018;85:201–20. doi:10.1016/j.engfailanal.2017.11.013.

[46] Milani G, Lourenço PB. A discontinuous quasi-upper bound limit analysis approach with sequential linear programming mesh adaptation. Int J Mech Sci 2009;51:89–104. doi:10.1016/j.ijmecsci.2008.10.010.

[47] Milani G. Upper bound sequential linear programming mesh adaptation scheme for collapse analysis of masonry vaults. Adv Eng Softw 2015;79:91–110. doi:10.1016/j.advengsoft.2014.09.004.

[48] Chiozzi A, Milani G, Tralli A. A Genetic Algorithm NURBS-based new approach for fast kinematic limit analysis of masonry vaults. Comput Struct 2017;182:187–204. doi:10.1016/j.compstruc.2016.11.003.

[49] Rotunno T, Fagone M, Bertolesi E, Grande E, Milani G. Single lap shear tests of masonry curved pillars externally strengthened by CFRP strips. Compos Struct 2018;200:434–48. doi:10.1016/j.compstruct.2018.05.097.

[50] Grande E, Fagone M, Rotunno T, Bertolesi E, Milani G. Coupled interface-based modelling approach for the numerical analysis of curved masonry specimens strengthened by CFRP. Compos Struct 2018;200:498–506. doi:10.1016/j.compstruct.2018.05.118.

[51] Bertolesi E, Milani G, Fagone M, Rotunno T, Grande E. Micro-mechanical FE numerical model for masonry curved pillars reinforced with FRP strips subjected to single lap shear tests. Compos Struct 2018;201:916–31. doi:10.1016/j.compstruct.2018.06.111.

[52] Basilio I, Fedele R, Lourenço PB, Milani G. Assessment of curved FRP-reinforced masonry prisms: Experiments and modeling. Constr Build Mater 2014;51:492–505. doi:10.1016/j.conbuildmat.2013.11.011.

[53] CNR DT 200/R1. Guidelines for the design and construction of externally bonded FRP systems for strengthening existing structures. 2013.

[54] Fagone M, Rotunno T, Bati SB. The Groin Vaults of St. John Hospital in Jerusalem: An Experimental Analysis on a Scale Model. Int J Archit Herit 2016. doi:10.1080/15583058.2016.1158331.

[55] Lubliner J, Oliver J, Oller S, Oñate E. A plastic-damage model for concrete. Int J Solids

Struct 1989. doi:10.1016/0020-7683(89)90050-4.

[56] Milani G, Esquivel YW, Lourenço PB, Riveiro B, Oliveira D V. Characterization of the response of quasi-periodic masonry: Geometrical investigation, homogenization and application to the Guimarães castle, Portugal. Eng Struct 2013;56:621–41. doi:10.1016/j.engstruct.2013.05.040.

[57] Milani G, Lourenço PB. Monte Carlo homogenized limit analysis model for randomly assembled blocks in-plane loaded. Comput Mech 2010;46:827–49. doi:10.1007/s00466-010-0514-0.

[58] Van der Pluijm R. Material properties and its components under tension and shear. 6th Can Mason Symp 1992. doi:10.1371/journal.pone.0003011.

[59] Pluijm R Van der, Rutten H, Ceelen M. Shear behaviour of bed joints. 12th Int. Brick/Block Mason. Conf., 2000. doi:10.1016/j.ifacol.2015.06.144.

[60] PAGE A. THE BIAXIAL COMPRESSIVE STRENGTH OF BRICK MASONRY. Proc Inst Civ Eng 1981. doi:10.1680/iicep.1981.1825.

[61] Dhanasekar M, Kleeman PW, Page AW. BIAXIAL STRESS-STRAIN RELATIONS FOR BRICK MASONRY. J Struct Eng 1985. doi:10.1061/(ASCE)0733-9445(1985)111:5(1085).

[62] Page AW. An Experimental Investigation of the Biaxial Strength of Brick Masonry. 6th Int Brick Mason Conf 1982.

[63] Milani G, Tralli A. A simple meso-macro model based on SQP for the non-linear analysis of masonry double curvature structures. Int J Solids Struct 2012;49:808–34. doi:10.1016/j.ijsolstr.2011.12.001.

[64] Milani G, Lourenço PB. 3D non-linear behavior of masonry arch bridges. Comput Struct 2012;110–111:133–50. doi:10.1016/j.compstruc.2012.07.008.

[65] Milani G, Rossi M, Calderini C, Lagomarsino S. Tilting plane tests on a small-scale masonry cross vault: Experimental results and numerical simulations through a heterogeneous approach. Eng Struct 2016;123:300–12. doi:10.1016/j.engstruct.2016.05.017.

[66] Milani G, Lourenço PB. Simple homogenized model for the nonlinear analysis of FRP-strengthened masonry structures. I: Theory. J Eng Mech 2013;139:59–76. doi:10.1061/(ASCE)EM.1943-7889.0000457.

[67] Bertolesi E, Milani G, Lourenço PB. Implementation and validation of a total displacement non-linear homogenization approach for in-plane loaded masonry. Comput Struct 2016;176:13–33. doi:10.1016/j.compstruc.2016.08.001.

[68] Heyman J. The stone skeleton: Structural engineering of masonry architecture. 2014. doi:10.1017/CBO9781107050310.

[69] Heyman J. ESTIMATION OF THE STRENGTH OF MASONRY ARCHES. Proc Inst Civ Eng (London) Part 1 - Des & Constr 1980;69:921–37.

[70] Su Y, Wu C, Griffith MC. Modelling of the bond-slip behavior in FRP reinforced masonry. Constr Build Mater 2011. doi:10.1016/j.conbuildmat.2010.06.021.

[71] Kashyap J, Willis CR, Griffith MC, Ingham JM, Masia MJ. Debonding resistance of FRP-to-clay brick masonry joints. Eng Struct 2012. doi:10.1016/j.engstruct.2012.03.032.

[72] Freddi F, Sacco E. A damage model for a finite thickness composite interface accounting for in-plane deformation. Eng Fract Mech 2016. doi:10.1016/j.engfracmech.2016.06.001.

[73] Oliveira D V., Basilio I, Lourenço PB. Experimental Bond Behavior of FRP Sheets Glued on Brick Masonry. J Compos Constr 2011. doi:10.1061/(ASCE)CC.1943-5614.0000147.

[74] Carloni C, Focacci F. FRP-masonry interfacial debonding: An energy balance approach to determine the influence of the mortar joints. Eur J Mech A/Solids 2016. doi:10.1016/j.euromechsol.2015.08.003.

[75] Capozucca R. Experimental FRP/SRP-historic masonry delamination. Compos Struct 2010. doi:10.1016/j.compstruct.2009.09.029.

[76] Ceroni F, Ferracuti B, Pecce M, Savoia M. Assessment of a bond strength model for FRP reinforcement externally bonded over masonry blocks. Compos Part B Eng 2014. doi:10.1016/j.compositesb.2014.01.028.

[77] Ghiassi B, Marcari G, Oliveira D V., Lourenço PB. Numerical analysis of bond behavior between masonry bricks and composite materials. Eng Struct 2012. doi:10.1016/j.engstruct.2012.05.022.

[78] Ghiassi B, Oliveira D V., Lourenço PB, Marcari G. Numerical study of the role of mortar joints in the bond behavior of FRP-strengthened masonry. Compos Part B Eng 2013. doi:10.1016/j.compositesb.2012.10.017.

[79] Ghiassi B, Silva SM, Oliveira D V., Lourenço PB, Bragança L. FRP-to-Masonry bond durability assessment with infrared thermography method. J Nondestruct Eval 2014. doi:10.1007/s10921-014-0238-8.

[80] Grande E, Imbimbo M, Sacco E. Numerical investigation on the bond behavior of FRCM strengthening systems. Compos Part B Eng 2018. doi:10.1016/j.compositesb.2018.03.010.

[81] Grande E, Milani G. Modeling of FRP-strengthened curved masonry specimens and proposal of a simple design formula. Compos Struct 2016;158:281–90. doi:10.1016/j.compstruct.2016.09.017.

[82] Grande E, Milani G. Interface modeling approach for the study of the bond behavior of FRCM strengthening systems. Compos Part B Eng 2018;141:221–33. doi:10.1016/j.compositesb.2017.12.052.

[83] Grande E, Imbimbo M. A simple 1D-Finite Element approach for the study of the bond behavior of masonry elements strengthened by FRP. Compos Part B Eng 2016. doi:10.1016/j.compositesb.2016.02.005.